ENGINEERING-PDH.com
ONLINE CONTINUING EDUCATION

FATIGUE ASSESSMENT OF CARBON FIBER REINFORCED POLYMER REPAIRED STEEL

Main Category:	Materials Engineering
Sub Category:	-
Course #:	MAT-123
Course Content:	59 pgs
PDH/CE Hours:	4

OFFICIAL COURSE/EXAM

(SEE INSTRUCTIONS ON NEXT PAGE)

WWW.ENGINEERING-PDH.COM
TOLL FREE (US & CA): 1-833-ENGR-PDH (1-833-364-7734)
SUPPORT@ENGINEERING-PDH.COM

MAT-123 EXAM PREVIEW

- TAKE EXAM! -

Instructions:

- At your convenience and own pace, review the course material below. When ready, click "Take Exam!" above to complete the live graded exam. (Note it may take a few seconds for the link to pull up the exam.) You will be able to re-take the exam as many times as needed to pass.
- Upon a satisfactory completion of the course exam, which is a score of 70% or better, you will be provided with your course completion certificate. Be sure to download and print your certificates to keep for your records.

Exam Preview:

1. According to the reference material, both Lagrangian and Eulerian formulations were used in this study to allow for small and large deformations, as needed
    a. True
    b. False
2. Using Table 2. Material and geometric model properties, what was the Modulus of Elasticity (E) for the composite patch used in the tests?
    a. 71 GPa
    b. 150 GPa
    c. 200 GPa
    d. 208 GPa
3. Crack propagation evaluation was based on the Paris Law. The Paris law represents the crack-growth-rate data as a parabolic line when plotted on a log-log scale.
    a. True
    b. False
4. According to the Modeling section of the reference material, the plate dimensions were 1000×500×10 mm, while CFRP and adhesive strips both had dimensions of 500×50 mm, with thicknesses of 1.2 and 1.0 mm, respectively. The two CFRP strips (as well as the adhesive strips) were centrally located with respect to the steel plate and were ___ mm apart from each other.
    a. 25
    b. 50
    c. 75
    d. 100

5. In order to evaluate the effect of prestressing on the CFRP, the CFRP patches were prestressed to a value of ___ MPa, for both single- and double-sided CFRP patches.
    a. 150
    b. 250
    c. 500
    d. 750
6. As expected, the double-sided prestressed CFRP-repaired models showed superior performance in comparison to other models. The results shown in Figure 24 demonstrated an improvement of up to __ times that of an unrepaired model for a water velocity angle at 0°
    a. 2
    b. 3
    c. 4
    d. 5
7. The water velocity, normal to the plate, was set to 20 mm/sec and it was based on a typical river flow velocity.
    a. True
    b. False
8. Using Table 5. Results Summary, what was the improvements of repaired plates compared to no CFRP for a double-sided patch at a water velocity angle 60°?
    a. 5.05
    b. 6.55
    c. 5.03
    d. 5.43
9. According to the reference material, double-sided CFRP repairs exhibit significant improvement over single-sided CFRP repairs, up to __ times.
    a. 2.3
    b. 2.7
    c. 3.1
    d. 3.6
10. Based on the adhesive material model, the yield stress was approximated as 30 MPa; therefore, if the von Mises stress exceeded 30 MPa, then the adhesive is said to have failed and the CFRP peeled.
    a. True
    b. False

Abstract

The Nation's Steel Hydraulic Structures (SHS) are suffering from significant deterioration due to various effects including corrosion, fatigue cracking, impact, and overloads. Current conventional methods used for the repair of steel bridges are accepted as the state-of-practice for the repair of SHS. However, the application of such methods to SHS has often proven to be ineffective as a result of the excessive deterioration present in the structures. The bridge-based crack repair methods were developed primarily for mitigating cracks under Mode I loading, while SHS often experience mix-mode cracking. Therefore, the need for developing repair methodologies that are pertinent to SHS is not just necessary but essential.

This report presents the numerical model constructed using a Coupled Eulerian-Lagrangian (CEL) analysis to calculate the stress intensity factors for different repair configurations. The methodology developed to extract the stress intensity factors from an explicit numerical model is also discussed. The model was successful in predicting the experimental results of water hitting a metal plate conducted by Ramsden (1996). Results show that CFRP-repaired plates show significant improvement over non-repaired plates and double-sided prestressed CFRP repairs exhibited the best performance, showing improvements of 5 times or greater compared to unrepaired models, and 2.5 to 3 times better results than single-prestressed and single-sided CFRP repairs.

Contents

Figures and Tables

Figures

Tables

Preface

This study was conducted for the Information Technology and Coastal and Hydraulics Laboratories under Monitoring Completed Navigation Projects (MCNP) Research Program, Innovative Methods for Crack Repairs Work Unit. The technical monitor was Dr. Guillermo A. Riveros.

The work was performed by Prof. Hussam N. Mahmoud from Colorado State University at Fort Collins, Colorado and Dr. Guillermo A. Riveros, Computational Analysis Branch of the Computation Science and Engineer Division, U.S. Army Engineer Research and Development Center – Information Technology Laboratory (ERDC-ITL). At the time of publication, Elias Arredondo was Chief, Computational Analysis Branch (CEERD-IE-C); Dr. Robert Wallace was Chief, Computation Science and Engineer Division (CEERD-IE); and David Richards, CEERD-IV-T was the Technical Director for ERDC-ITL. The Deputy Director of ERDC-ITL was Patti Duett and the Director was Dr. Reed L. Mosher.

COL Jeffrey R. Eckstein was the Commander, ERDC, and Dr. Jeffery P. Holland was the Director.

Executive Summary

The Nation's steel hydraulic structures (SHS) are suffering from significant deterioration due to various effects including corrosion, fatigue cracking, impact, and overloads. Current conventional methods used for the repair of steel bridges are accepted as the state-of-practice in the repair of SHS; however, the application of such methods to SHS has often proven to be ineffective as a result of the excessive deterioration present in the structures. Furthermore, the bridge-based crack repair methods were developed primarily for mitigating cracks under Mode I loading, while SHS often experience a combination of various loading modes. The need for developing repair methodologies that are pertinent to SHS is ever-pressing. If properly applied, the use of Carbon Fiber Reinforced Polymer (CFRP) composites for the repair of fatigue cracks can result in a significant increase in fatigue life.

The aim of this study is to evaluate the effectiveness of CFRP patches for the repair of SHS. This is realized through conducting a coupled Eulerian-Lagrangian (CEL) finite element simulations of repaired panels subjected to moving water. A parametric study of single-sided and double-sided CFRP patch repairs of steel panels was conducted to examine their effectiveness. The retrofitted panels are subjected to a moving body of water which interacts with the panel and the CFRP patches. Different boundary conditions are investigated in the simulations to represent both open and closed miter gate condition. Furthermore, the applied boundary conditions are representative of what might be observed in actual field conditions. Various other parameters that were considered in the simulations included crack length, prestressing of CFRP patches, different water impact angles, and single-sided versus double-sided CFRP repairs. The results show significant improvement in reducing the crack propagation and increasing fatigue life for up to approximately eight times that of the unrepaired conditions. This is especially the case for double-sided retrofit with and without prestressing. The single-sided repair, although a viable option, has an effectiveness that is reduced to the asymmetrical axial load introduced in the repair, which results in an added moment that aggravates the crack opening condition on one side of the plate.

1 Introduction

Steel hydraulic structures (SHS) such as locks, spillway gates, and maintenance closure structures may have fabrication defects and flaws that can be large enough to threaten the integrity of the structure. In addition to fabrication defects and flaws, the Nation's SHS are suffering significant deterioration caused by the combined effects of several complex phenomena including corrosion, cracking and fatigue, impact, and overloads (Riveros and Arredondo 2010). Structural systems are also suffering from deterioration of design boundary conditions. Examples of SHS with existing flaws, fatigue crack, and significant deterioration are shown in Figure 1. Specifically, Figure 1(a) shows an existing torch-cut drain hole of a bulkhead, which could be a source of crack initiation. Figure 1(b) shows significant corrosion in a miter gate. Figure 1(c) shows an edge fatigue crack, which developed at the end of a bearing pad of a bulkhead. Other common defects in SHS include incomplete joint penetration, center cracks, buried penny-shaped cracks, pitting corrosion; among other defects (Dexter et al. 2007). Examples of deterioration of boundary conditions induced cracking are shown in Figure 1(d) and Figure 1(e).

Figure 1. Failure modes of miter gates

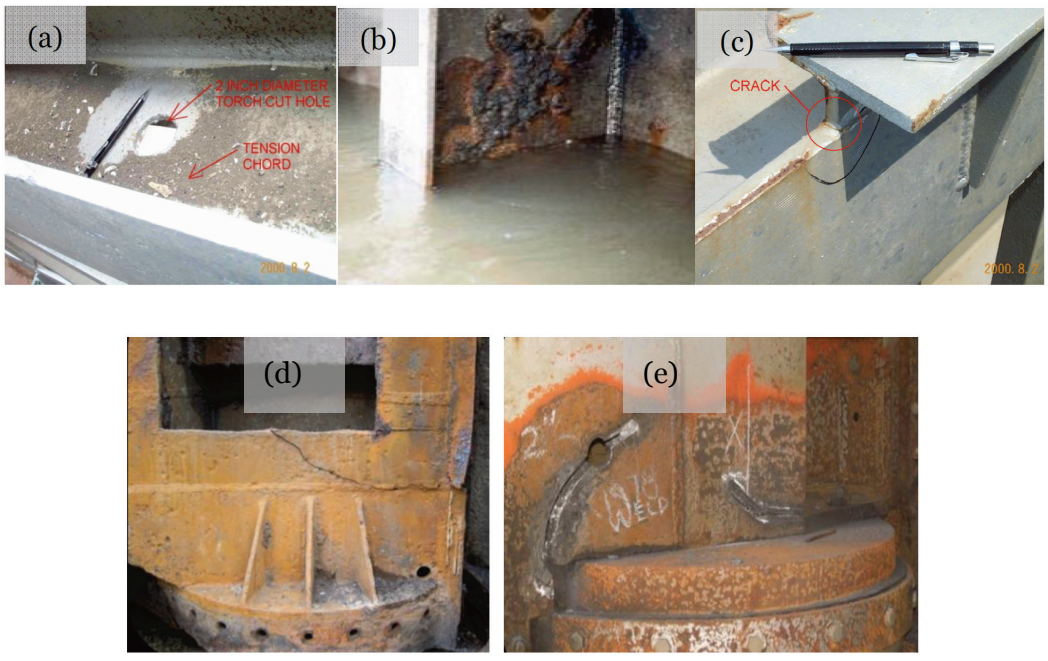

1.1 Background

The current conditions of SHS can threaten the integrity of the structure and need to be continuously inspected and repaired. Effective and economical retrofit practices are essential for ensuring continuous operation and mitigation for the level of risk associated with possible catastrophic failure. Current methods of repair for SHS are adopted primarily from the bridge engineering industry. These repair methods have proven to be ineffective in many cases because of excessive corrosion and deterioration conditions of the SHS, and in some cases to differences in operation and loading conditions. In addition, the cost and time associated with the implementation of conventional repair methods can be rather significant.

Carbon Fiber Reinforced Polymer (CFRP) sheets for the repair of steel structures offer significant potential as a repair alternative due to the light weight, durability, and excellent fatigue and corrosion resistance characteristics, as demonstrated by recent research studies. However, the applicability to SHS is still unclear because previous studies conducted on steel in dry environments gave no attention to the impact of wet environments on the effectiveness of CFRP repairs. Preliminary evaluation of previous experimental, numerical, and analytical studies clearly show that research is needed to investigate the applicability of using CFRP for the repair of fatigue cracks and corrosion fatigue in SHS.

Particularly, research needs to focus on characterizing the effect of the wet environment and corrosion on the propagation rate of cracks as they interact with the CFRP patches. A debonding model of the CFRP patches, which accounts for the crack length, level of corrosion, and the time of exposure to a wet environment, appears to be lacking. Moreover, the models should include the effect of freeze and thaw cycles on the fundamental characteristics of the adhesive and debonding mechanism. This is an important issue since SHS are operated in hot and freezing conditions.

1.2 Previous Studies on CFRP-Repaired Steel Elements

Various studies have been carried out to assess the use of CFRP for the rehabilitation of the increasingly aging and deteriorated civil structures and infrastructure systems in the United States. The deterioration is typically manifested in terms of fatigue cracking or corrosion cracking. Most previously conducted studies were aimed at investigating the use of CFRP

for flexure and shear retrofitting of concrete structures (Maruyama 1997; Meier and Betti 1997; Neale and Labossiere 1997; Taljsten 1997; Benmokrane and Rahman 1998; Thomas 1978; Triantafillou 1998; Mirmiran et al. 2004). The studies highlighted the significant potential of such an application as demonstrated by the numerous field implementations of CFRP repair of concrete structures. Much less research has been conducted on the use of CFRP in strengthening metallic structures with most studies geared towards flexure retrofitting of aluminum panels in the aviation industry (ASCE Committee on Composite Construction 2006); therefore, it is not surprising that field implementation of CFRP composites for retrofitting steel structures is scarce. In general, research efforts on retrofitting steel elements has examined the following areas; (1) repair of naturally deteriorated steel girders; (2) repair of an artificially notched girder or steel plates to simulate fatigue cracks; (3) strengthening an intact section to increase the girder stiffness and flexural capacity; and (4) increasing the composite action between the steel girder and concrete deck in bridge application (Shaat et al. 2004).

Experimental and analytical studies on investigating crack growth of adhesively repaired steel panels were conducted on flat steel specimens and have shown an increase in fatigue life in comparison to the unrepaired specimens (Young and Roore 1992; Colombi et al. 2003; Jones and Civjan 2003; Duong and Wang 2004; Yue et al. 2004; Hansen et al. 2007; Liu et al. 2009). Very few studies have been conducted on fatigue crack propagation in CFRP-repaired large scale specimens representing real structural members (Bassetti et al. 1999; Mertz et al. 2002; Tavakkolizadeh and Saadatmanesh 2003; Jiao and Zhao 2004; Shield et al. 2004; Vatandoost 2010; Kim and Harries 2011). Although in some of the large scale studies, the conclusion on fatigue life improvement is not clearly discussed. It can be generally concluded that a 3-7 folds increase in fatigue life was observed for retrofitted specimens when compared to their unretrofitted counterparts.

1.2.1 Previous Analytical Studies

Measurable effort has been undertaken to develop numerical finite element models for the assessment of cracked metals patched with CFRP. Various modeling techniques have been investigated and their results compared in order to develop the most accurate and economical models. The models vary from pure 3D continuum formulations of the steel, adhesive, and CFRP patch using continuous elements to 2D continuum formulations of the steel

and CFRP patch, which are linked with spring or beam elements to simulate the bonding effect. The fundamental challenge pertaining to modeling the plate-adhesive-CFRP system is in characterizing the 3D stress flow path in the system (Umamaheswar and Singh 1999). The problem is further aggravated for one-sided patches, which result in out-of-plane deformation and large localized rotations (Umamaheswar and Singh 1999).

The summary below is aimed at highlighting the most relevant studies on analytical and numerical models developed to evaluate fatigue crack propagation in CFRP-bonded steel elements. A more comprehensive overview of the background on existing models can be found in Mahmoud and Riveros (2013).

Chue et al. (1994) investigated the performance of bonded repairs of a plate containing an inclined central through-thickness crack under a biaxial loading effect. The goal of the analysis was to optimize the orientation of the bonded repair using single- or double-sided patches, so that the maximum adhesive shear stress and the patch fiber stress meet the design requirements. The analysis was conducted using a 3D finite element method (FEM) with 20-noded brick elements with the region adjacent to the crack front being modeled using singular crack elements. The singular elements were used to introduce the required stress singularity by shifting the side nodes to the quarter point position. The results were validated against existing analytical solutions and the error was found to be approximately 11 percent. For more effective repairs, the authors suggested that fiber orientation should coincide with the maximum tensile load direction in a double-sided patch and perpendicular in the case of a single-sided patch.

Sun et al. (1996) introduced a new 2D model called “the three-layer technique” to analyze the repair of thin cracked aluminum structures bonded to a CFRP patch. The model was introduced as a cost-effective alternative to 3D finite element models, which are computationally expensive and difficult to construct. As its name implies, the model was comprised of three layers representing the cracked plate, the adhesive, and the composite patch. In this model, the aluminum plate and the CFRP patch were modeled using a Mindlin plate element and the adhesive layer was modeled using an effective spring. The model was developed using ABAQUS and was used to evaluate the behavior of the retrofitted panels under different levels of biaxial loading conditions represented by the ratio

of the axial and transverse stresses ($\lambda = \sigma_x/\sigma_y$). For two-sided repair, the proposed model provided excellent agreement with boundary element solutions and 3D finite element models for the calculated stress intensity factors (SIF). However, for a single-sided repair, large discrepancies were present. This could be due to the use of spring elements to represent the adhesive, which are not capable of transferring the moment introduced by the asymmetric conditions as a result of the repair being one-sided. The in-plane shear stiffness (i.e., x and y) and the axial (peel) stiffness of the springs can be determined using equation (1) and (2), respectively.

$$k_{x,y} = G_a A / t_a \tag{1}$$

$$k_x = \frac{2(1-\nu_a)G_a A}{(1-2\nu_a)t_a} \tag{2}$$

Where G_a is the adhesive shear modulus, t_a is the adhesive thickness, A is the area represented by the shear spring, and ν_a is the adhesive Poisson's ratio.

Naboulsi and Mall (1996) utilized the "three-layer technique" to analyze the fatigue behavior of a repaired panel subjected to different levels of biaxial loading conditions represented by $\lambda = \sigma_x/\sigma_y$. In this study, all constituents were modeled using plate elements with shear capabilities. The results of the analysis were in good agreement with previously published results of 2D models where the adhesive is simulated using spring elements. The authors verified the three-layer technique later against experimental fatigue results of cracked aluminum panels repaired with imperfectly bonded CFRP patches. The results showed strong correlation between the finite element models and experiments. Various reasons might contribute to not having an excellent match between the finite element and experimental results including, for the example, the inaccurate representation of the bond shear stiffness using the spring elements.

The results of all three models are listed in Tables 1 and 2, providing insight on the accuracy of the models. The comparison highlights the efficiency of the 2D models as all four models yielded similar results. There is, however, stronger agreement between the 3D Chue et al. (1994) and the 2D Sun et al. (1996) models and between the 3D Sun et al. (1996) and the 2D Naboulsi and Mall (1996) models.

Table 1. Comparison of force results between experimental and numerical modeling.

Velocity (m/s)	Contact-Stiffness Force $1550v\sqrt{m}$ (N)	Numerical Modeling Force (N)	Difference
0.381	2,621	3,218	54.3%
0.533	3,667	3,218	12.2%
0.800	5,504	4,037	26.6%

Table 2. Material and geometric model properties

	Length L (mm)	Width W (mm)	Thickness h (mm)	Material Properties
Aluminum Plate	180	120	2.2900	E = 71.02 GPa ν = 0.32
Adhesive	76	38	0.1016	G = 0.965 GPa ν = 0.32
Composite Patch	76	38	0.7620	E_1 = 208 GPa $E_1 = E_2$ = 25.44 GPa G_{23} = 4.94 GPa $G_{12} = G_{13}$ = 7.24 GPa ν_{23} = 0.035 $\nu_{12} = \nu_{13}$ = 0.1677

Schubbe and Mall (1999) conducted a combined experimental and analytical study to evaluate fatigue crack growth behavior of thick aluminum panels repaired asymmetrically with an adhesively bonded composite patch. The experimental results showed that the one-sided repair resulted in nonuniform crack propagation with an elliptical crack front. Debonding of the patch occurred in the vicinity of the crack with an elliptical debonding shape. The finite element models were developed using the 2D three-layer model with plate elements to evaluate the fatigue crack growth in the plates. The difference in the crack size on both sides of the plates was incorporated in the models by adjusting the crack length, using a linear crack assumption, to account for the lag between the midplane and unpatched face.

Umamaheswar and Singh (1999) investigated various finite element modeling techniques to CFRP-patch repair of aluminum panels with an edge crack. The models were developed using the commercial code "Numerically Integrated Elements for Systems Analysis (NISA)." The

model comprised of four-noded general shell elements for the panel and CFRP and general beam elements for the adhesive. The reason for modeling the adhesive using beam elements as opposed to spring elements, as in the case of the work by Naboulsi and Mall (1996), was because spring elements were not available within NISA. The elements were first-order linear elements, which cannot handle singularity at the crack tips; therefore, the stress intensity factor at the crack tip was estimated using a modified crack closure integral method. The results of the analysis were promising because the models yielded SIF values that were within 4-5 percent of full 3D models and resulted in significantly reduced computational time. However, the issue with this type of model is typically the time required to set up the material properties of the beam/spring elements used to model the adhesive. It should be noted that an error of 4-5 percent in estimating the solution for the SIF is considered acceptable and will not have much impact on the overall results.

In the same study, Umamaheswar and Singh (1999) developed a 2D/3D plate-brick model where the panel and the CFRP patch are modeled using a four-noded shell element and the adhesive model using brick elements. The benefit of modeling the adhesive using brick elements is to provide a continuous attachment between the two adherents. The authors indicated that this modeling approach overestimates the strain energy release rate, as the corresponding nodes on the panel and patch are not directly linked. It is, however, unclear as to the reason for having an incompatible deformation field between the adherents. The authors also developed a full 3D brick model as part of this study. In this model, only one brick was used across the panel, the adhesive, and the CFRP patch. In doing so, the size of the model was very comparable to the 2D shell-spring/beam-spring model, resulting in a comparable overall computation time between the two models. The 3D brick model provided results that are in closer agreement with the reference solution with an error of only 1.0 – 1.5 percent.

Colombi et al. (2002) utilized the three-layer technique, using the finite software ABAQUS, to evaluate the effect of CFRP prestressing on the propagation of short and long cracks in retrofitted steel plates. The model utilized shell elements for the steel plate, the adhesive, and the CFRP patch. Constraint equations were used to enforce compatibility along the plate-adhesive and adhesive-patch interface. The debonded crack was modeled at the plate-adhesive interface with a semi-elliptical shape. The analysis was performed for different delamination sizes but the propagation of the

delamination was not modeled. The results indicated that for long cracks, the CFRP strips modified the geometry as they bridge the crack lips, while for short cracks, the effect of the patch is evident in reducing the stress range. Moreover, the effect of the repair decreases as the thickness of the adhesive decreases. This is because of the large shear deformation imposed on thin adhesives. For long cracks, the effect of shear deformation in the adhesive is important since the ability of the CFRP strips to effectively bridge the crack lips is reduced by shear deformation in the adhesive. For short cracks outside of the patch area, the deformation in the adhesive is not important. The effect of CFRP prestressing on the calculated SIF was evident in the study where the applied SIF range remained unchanged but the stress ratio decreased. The reduction in the stress ratio will promote crack closure and result in reduction in the crack growth rate.

Seo and Lee (2002) used ABAQUS to develop a model to evaluate crack propagation in aluminum panels repaired with CFRP. The model comprised of 20-node brick elements for the panel, the adhesive, and the patch. Quarter point crack tip singularity elements were used to model the crack tip. The authors noted, based on experimental results, that for thick specimens and for one-sided repair, there is a considerable crack front growth variation between the patched and unpatched sides, which are similar to the observation made by Schubbe and Mall (1999). The one-sided patch resulted in an elliptical crack front with crack variation between both sides of approximately 10 mm (0.39 in.) for 30 mm (1.18 in.) crack lengths. The elliptical crack front was idealized as a linear skew variation in the model for simplicity. The finite element results showed large variation in the SIF in the through thickness direction with higher values obtained on the unpatched side than the patched side. Several average values in the through thickness direction were obtained. Good correlation was obtained between the experimental results and the root mean square of all through thickness values, and the average values from the unpatched side to mid-plane. The authors indicated that the predicted fatigue life is a function of the SIF averaging method of the through thickness values. The root mean square of all through thickness values and the averaged values to mid-plane can be considered as the lower and upper bound values for estimating the SIF.

Hosseini-Toudeshky and Mohammadi (2007) used the commercial finite element code ANSYS (2014) to model crack growth in aluminum panels, retrofitted on one side with composite patches. Isotropic 8-node solid

elements were used for the panel, the adhesive, and the patch. Crack growth analysis was conducted using a uniform crack growth approach and a nonuniform (i.e., elliptical) crack growth approach. It was found that the uniform crack growth method resulted in an unconservative fatigue life on the order of 35-90 percent as compared to experimental results. The elliptical crack propagation method, however, resulted in a fatigue life estimate that is reasonably accurate (within 10 percent of experimental results). The elliptical crack propagation method is rather complicated and requires the crack shape to be adopted in the analysis. The authors proposed a new and simple position for estimating the SIF value along the panel thickness, which results in a fatigue life estimate that is very comparable to that obtained using the elliptical propagation approach. In other words, propagating the crack in a uniform way up until that position will result in an accurate life estimate as compared to the elliptical crack propagation method.

It is important to note that all of the above mentioned studies were conducted on CFRP-retrofitted steel elements exposed to in-air conditions, and therefore, deviation from these results in reference to SHS is rather expected. This is because SHS often suffer from extreme corrosion caused by their continuous exposure to the wet environment, which results in significantly earlier fatigue crack initiation and higher rate of propagation when compared to steel in-air. Accelerated debonding can be expected when the plate-adhesive-CFRP system is subjected to water. Furthermore, only geometries under Mode-I loading were included in the studies. The reason for investigating Mode-I cracking is because most fatigue details in steel bridges are predominantly subjected to Mode-I cracking and the American Association of State Highways and Transportation Officials (AASHTO) fatigue S-N curves were developed based on this type of loading (AASHTO 2012). It is worth noting that current fatigue guidelines and provisions used for SHS are borrowed from the steel bridge industry.

Evidence has shown cracking to develop in SHS as a result of Mode-II cracking. Consequently, the extent of the applicability of existing AASHTO fatigue provisions, which were developed for steel bridges under Mode-I loading, to steel hydraulic structures is unclear. Furthermore, some bridge details are known to be subjected to Mode-II and III loading, and often develop some cracking. Existing repair methods for steel bridges, which are primarily based on Mode-I cracking, have proven to be ineffective when applied to details that have cracked under Mode-II or Mode-III. For

example, distortion-induced fatigue in steel bridges is known to develop because of the out-of-plane distortion of the bridge girder webs (Mode-III). The hole-drilling method that is generally effective for repairing cracks under Mode-I is often ineffective in mitigating the out-of-plane distortion cracking.

This brief discussion clearly demonstrates the need for alternative economical and effective methods for the repair of fatigue cracks in SHS. Repair methodologies utilizing CFRP composites can result in a significant increase in fatigue life if properly applied to SHS. The current state of practice and research, however, did not address many issues pertaining to the use of CFRP in wet and corrosive environments and under complex loading conditions. The presented study initiates the research of CFRP effectiveness for repairing cracks in SHS, by simulating wet conditions, applying realistic loading, and including effects such as corrosiveness and debonding.

2 Modeling

2.1 Coupled Eulerian-Lagrangian Modeling Technique and Model Parameters

Recent advancements in both hardware and software have permitted the construction of numerical models, which allow for accurate simulation of fluid-structure interaction (FSI) without the necessity of coupling the structural analysis tools with computational fluid dynamics capabilities. The models developed in this study were analyzed using the Coupled Eulerian-Lagrangian (CEL) analysis technique available in ABAQUS software (SIMULIA 2012). The Eulerian capability included in ABAQUS can be coupled with traditional Lagrangian formulations to model interactions between highly deformable materials and relatively stiff bodies, such as the fluid-structure interaction between water and miter gates (SIMULIA 2012). The convenience of the CEL formulation significantly reduces the analysis time for fluid-structure interaction problems that are otherwise very demanding if traditional computational fluid dynamics were to be used.

Both Lagrangian and Eulerian formulations were used in this study to allow for small and large deformations, as needed. The water was modeled as an Eulerian component, assuming a Newtonian, nearly incompressible and practically frictionless fluid. The general contact approach was implemented in ABAQUS as the contact formulation between water and the structural elements in the model. The general contact algorithm automatically computes and tracks the interface between the Lagrangian structure and the Eulerian materials, while penalty methods are used to couple the Eulerian and Lagrangian parts (ABAQUS Analysis User's Manual 2011). A surface-to-surface contact formulation with rough friction and no separation was used for contact between the Lagrangian parts. An overview of the finite element model as well as a view of the plate and CFRP mesh is shown in Figure 2.

With respect to the Lagrangian (structural) parts, three material models needed to be implemented. These included the steel, CFRP, and adhesive materials. The steel was modeled as a linear elastic material with E = 200 GPa and ν = 0.3. The CFRP patch was modeled as an orthotropic material (Naboulsi and Mall 1996; Bassetti et al. 1999), while the adhesive was

modeled as a linear elastic material. The adhesive model shown in Figure 3 was obtained by Riveros and Rosario (2013); the used parameters were E = 12.8 GPa and ν = 0.29. It is important to note that the use of elastic material properties is enforced since linear elastic fracture mechanics (LEFM) is used. While the elastic properties of the adhesive are used, an assessment can still be made as to whether the adhesive can withstand the applied strain.

Figure 2. Overview of the finite element model.

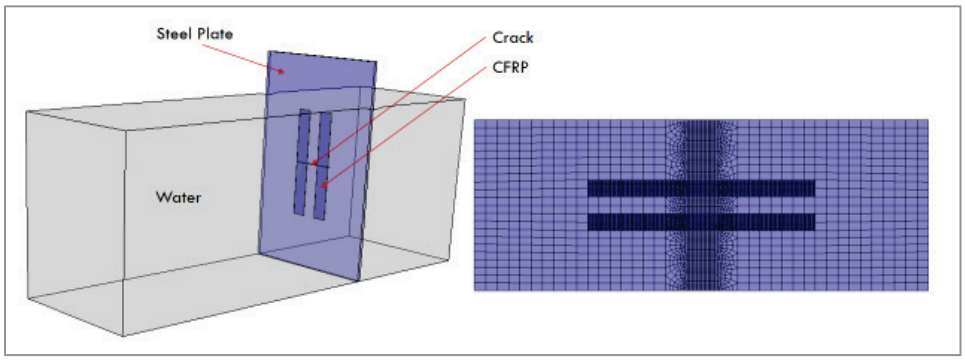

Figure 3. Adhesive Material Model (Riveros and Rosario 2013).

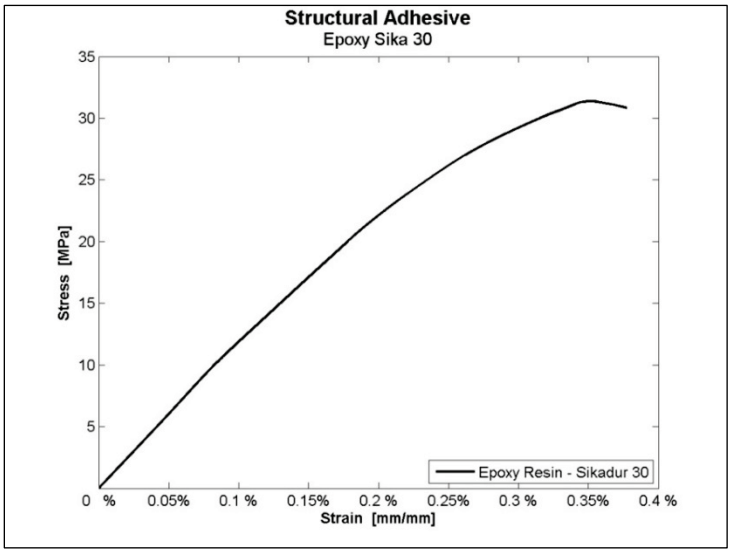

Based on the condition of gate operation, the plate boundary conditions change from the closed position to the open position. In the closed position, the plate is supported on both sides. At the bottom, the plate is supported by pinned connections, while at the top corners there are roller supports that inhibit the out-of-plane movement. While the gate is being operated to an open position, only one side of the plate is supported with similar connections to the closed case, pinned at the bottom, and

constrained out-of-plane motion at the top. Due to the different support cases between the gate being open and closed, adjustments in the plate boundary conditions during the analysis were implemented in order to realistically represent field conditions. A depiction of the boundary conditions is shown below in Figure 4.

Figure 4. Boundary conditions for closed and open conditions.

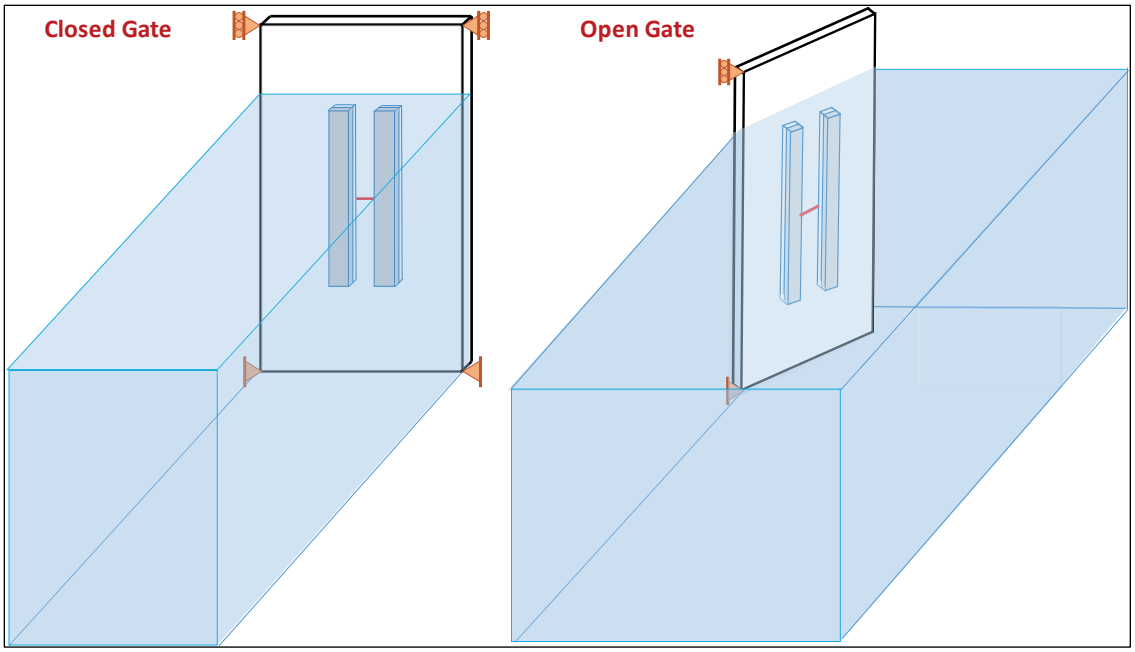

The plate dimensions were 1000×500×10 mm, while CFRP and adhesive strips both had dimensions of 500×50 mm, with thicknesses of 1.2 and 1.0 mm, respectively. The two CFRP strips (as well as the adhesive strips) were centrally located with respect to the steel plate and were 50 mm apart from each other.

2.2 Analysis Framework and Crack Propagation Modeling

The CEL analysis is implemented in ABAQUS through a dynamic, explicit analysis framework. While this analysis scheme is stable, it does not allow for direct evaluation of the stress intensity factor. Therefore, a procedure was developed to obtain the required *K* values such that LEFM can be used for determining the crack propagation rate. Figure 5 outlines the process of extracting the *K* values. The procedure starts by conducting a CEL analysis to determine the applied nodal deformations on all nodes in the model. The applied deformations are then extracted using a Python code at the frame corresponding to the maximum stresses. Once the

deformations are obtained, the input file corresponding to the dynamic analysis is modified where the elements representing the water are removed, the extracted deformations are inserted as initial conditions, and the analysis is converted into a static analysis.

Figure 5. Flow chart to obtain K_{max}.

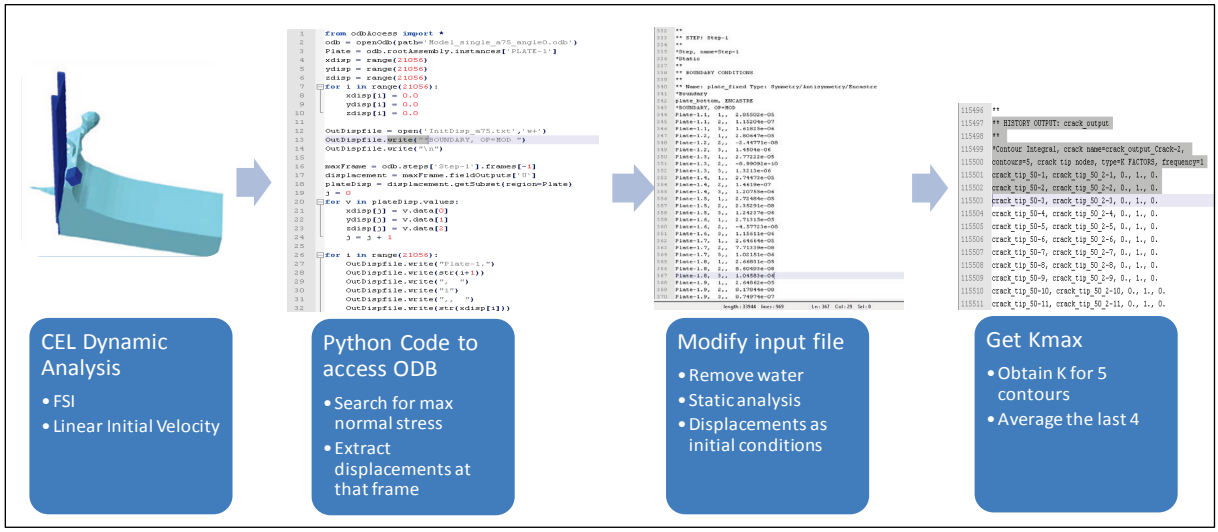

Crack propagation evaluation was based on the Paris Law. Paris hypothesized that the range in stress-intensity factor, ΔK, governs fatigue crack growth, (Paris and Erdogan 1963). The Paris law represents the crack-growth-rate data as a straight line when plotted on a log-log scale (Trask 2000). However, experimental *da/dN* verses ΔK data typically exhibit a sigmoid shape when plotted on a log-log scale. There is a ΔK threshold, ΔK_{th}, below which cracks will not propagate. ΔK_{th} can be taken as 3 MPa-m$^{1/2}$ for structural steel. The Paris Law is fit to the linear part (on a log-log scale) above ΔK_{th}. At relatively high ΔK levels, the crack growth rate accelerates accompanied by some ductile tearing or increments of brittle fracture in each cycle. The Paris Law is shown in Equation 3.

$$\frac{da}{dN} = C \bullet \Delta K^m \tag{3}$$

where a is half the crack length, N is the number of cycles, and C and m are material constants. For corrosive environments, $C=2.4 \cdot 10^{-12}$ $(mm \cdot cycles)(MPa \cdot \sqrt{mm})$ and $m = 3$, as recommended in British Standards (BS) 7910 (2012). ΔK is the range of the applied stress intensity factors.

$$\Delta K = K_{max} - K_{min} \tag{4}$$

It is assumed that K_{min} = 0, therefore, $\Delta K = K_{max}$. The assumption on K_{min} being equal to zero stems from the fact that when the gate is dewatered the applied pressure is essentially zero. The Paris Law is universally known to be valid only for Mode I cracking, therefore, only the stress intensity factor for mode I was evaluated ($K_I = \Delta K$). It should be noted that very limited studies have considered the application of the Paris Law to other modes.

In the static analysis, the calculation of the stress-intensity factor can be requested as an output parameter in ABAQUS. For the calculation of the stress intensity factor, five values were requested. An average of only the second, third, fourth, and fifth values were computed. This is because inaccuracies in the stresses at the row of elements immediately adjacent to the crack tip could yield higher error than subsequent contour paths.

3 Verification

3.1 CEL Methodology Verification

Verification efforts were focused on two fronts: overall model methodology (CEL and FSI methodology) and crack modeling. The CEL methodology used in this study has been verified through several benchmark problems such as the classical problem of a dam breaking, and comparisons to experimental studies, such as debris impact force on a wall due to tsunami loading (Como and Mahmoud 2013; Haehnel and Daly 2002) and water on a flume hitting an aluminum plate (Ramsden 1993).

For modeling of debris impact forces on a wall, a validation of the utilized CEL methodology was conducted based on previous experimental tests. Small-scale experimental tests of debris striking an isolated rigid wall have been conducted. One set of comprehensive tests was conducted by Haehnel and Daly (2002) in which small-scale flume tests were used to evaluate the force resulting from wood logs impacting a stationary target. Out of eight test series, selective tests were chosen to verify the modeling approach used in this numerical study, as they mimicked the same hydrodynamic conditions as the field conditions. In the actual experiments, logs of varying weight and cross-sectional dimensions were used to measure the impact forces on a stationary target. In addition to log weight, flow velocity, impact orientation, and target material were varied. The load frame had a 7.5 cm semi-circular target mounted on a front plate, which in turn was mounted on three load cells. The load cells were fastened to a rigid frame mounted on the flume floor (Haehnel and Daly 2002). The rounded target ensured that the point of impact is concentrated between the three load cells such that all of the load cells were in compression on impact. The corresponding finite element model used for verification was constructed using the exact experimental measurements and relative placements of debris, water, and load cell used by Haehnel and Daly (2002). Plan views of the experimental set-up and corresponding ABAQUS model are shown in Figure 6. The physical water-debris-wall interaction is shown in Figure 7.

Out of forty-eight different tests, three small-scale experiments were numerically modeled for verification purpose, which consisted of a reduced-scale log with a cross-section of 8×8 inches and length of 36 inches. Three different water velocities were selected from the actual experiments, mainly

0.381, 0.533, and 0.8 m/s. For estimating the impact force, three different approaches were utilized and included Contact-Stiffness, Impulse-Momentum, and Work-Energy approach. Out of the three mentioned approaches, only the Contact-Stiffness formulation is applicable to the small-scale flume tests. The obtained force results from the ABAQUS models compared fairly well against the Contact-Stiffness formulation and the individual recorded experimental results.

Figure 6. Experimental set-up (Haehnel and Daly 2002) (left) and finite element modeling (Como and Mahmoud 2013).

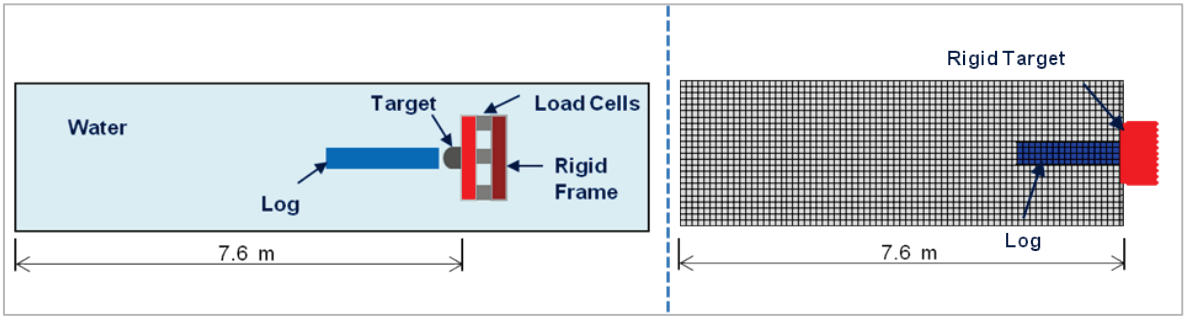

Figure 7. Water-debris-wall interaction (Mahmoud and Como 2013).

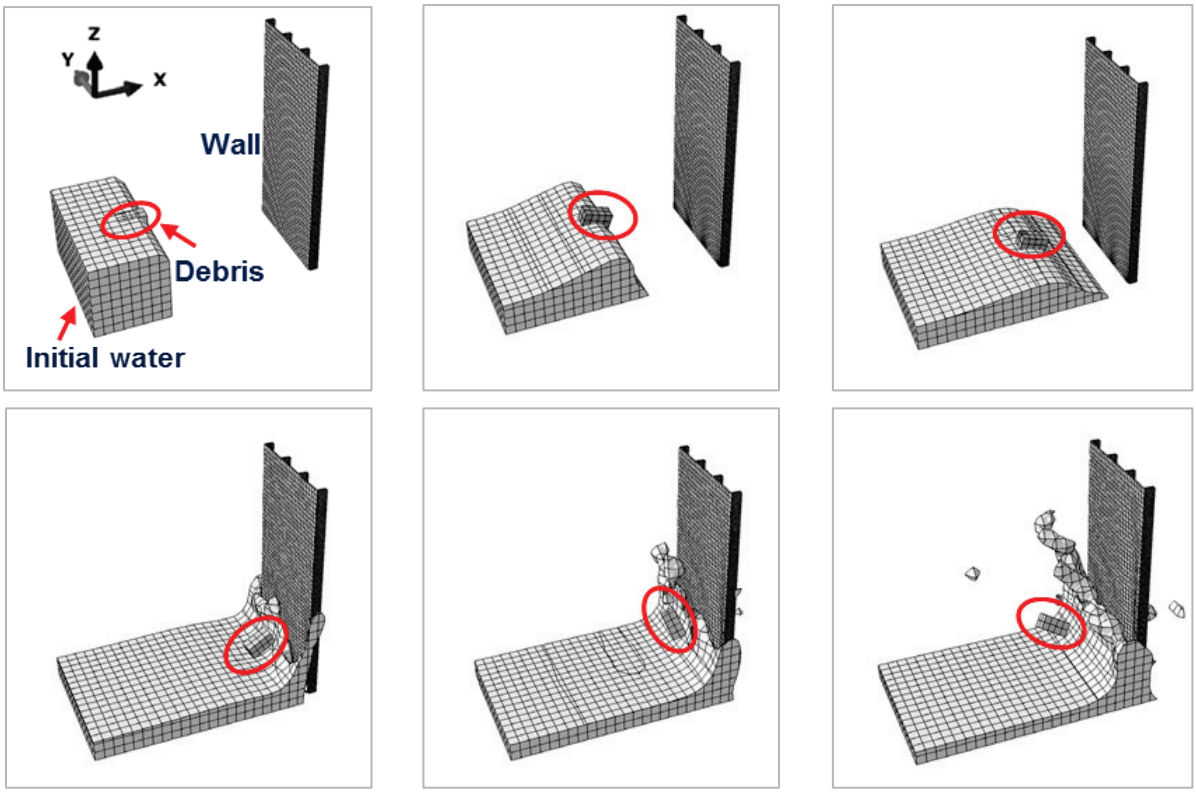

In terms of numerical force results, two of the obtained forces were within 12% and 27% of the expected values based on the Contact-Stiffness formulation, as presented in Table 1. Haehnel and Daly (2002) observed that the flume tests exhibited some scatter and the Contact-Stiffness formulation overestimated force for values less than 10 kN (which is the case in the small-scale experiments). This observation matches the numerical results, as illustrated in Figure 8. The numerical results are within the range of experimental results; thus, the validation of the approach is confirmed prior to conducting the parametric studies on the panels.

Figure 8. Validation of numerical results (Como and Mahmoud 2013; Haehnel and Daly 2002).

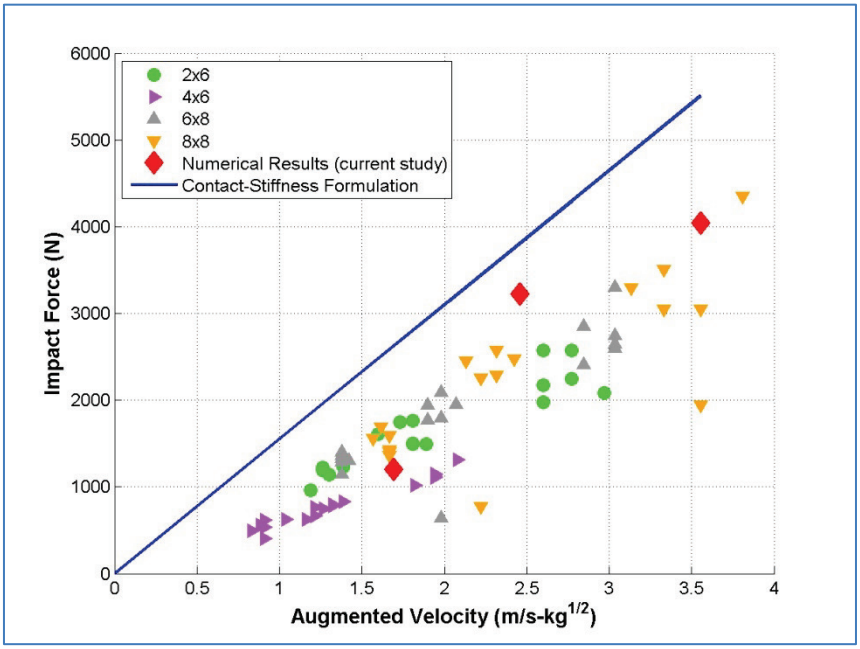

A third verification of the CEL method was completed by modeling water flowing through a flume and impacting a vertical aluminum plate. The conducted study consisted of experimental evaluation of forces and overturning moments on a vertical wall due to the reflection of solitary waves, undular bores, turbulent bores, and surges on a dry bed (Ramsden 1996). The tests were conducted in two wave tanks, a tilted wave tank and a horizontal wave tank. For modeling and analysis efficiency, one of the dry surge bed tests was used as a model for the constructed CEL finite element model. In the experimental study, a pneumatic gate was used to create bores and surges on a dry bed by releasing a volume of water in a reservoir as shown in (Ramsden 1996). In the numerical model, an initial volume of water similar to the dry bed surge was defined and gravity load

was applied to the model in order to mimic the sudden release of water. The experimental setup is shown in Figure 9 and the associated CEL finite element model is shown in Figure 10. As shown in both figures, the profile of the water upon impact is very similar.

Figure 9. Experimental Set-up (Ramsden 1996).

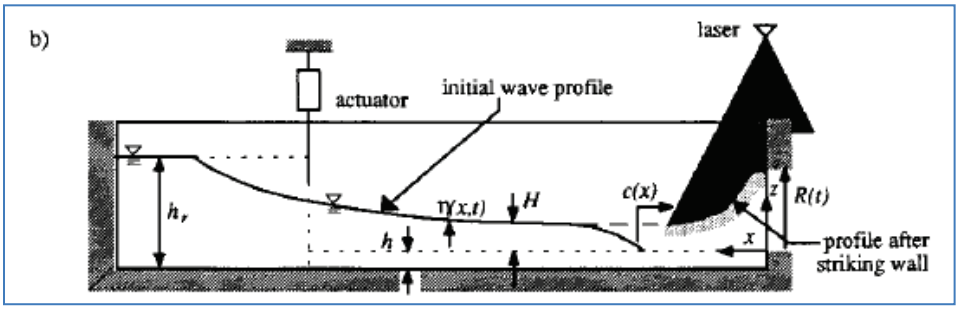

Figure 10. Initial and post-impact wave profile (Ramsden 1996).

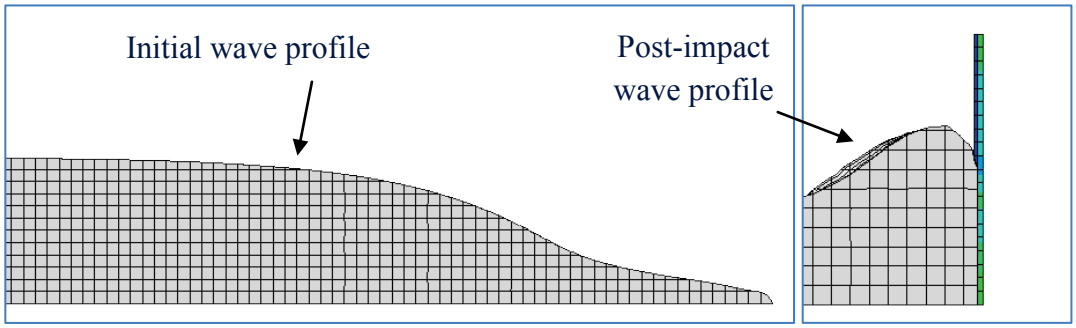

The instrumented section of the wall (center wall) was supported with four force transducers, which were mounted on the centerline of the wall at a distance of 7.7 cm, 21.4 cm, 34.9 cm, and 52.3 cm above the bottom of the tank cm, 21.4 cm, 34.9 cm, and 52.3 cm above the bottom of the tank (Ramsden 1996). In addition, the pressure transducer was mounted in one of five ports along the centerline of the wall. One of the five locations of the pressure transducers was located at 1.79 cm above the tank bottom. The modeled specimen is noted by HS86, and though finer mesh was required for accuracy, the resultant force per width was found to be in the same magnitude range as the corresponding experimental value. Specifically, the experiment force result is 465.4 N/m, while the numerical value is 350 N/m.

3.2 Crack Modeling Validation

Validation of crack modeling was achieved through evaluating the stress intensity factor (K) of a plate with a center crack subjected to normal

stress, and evaluating the normalized stress intensity factor of a plate with a center crack repaired with a single CFRP patch. The obtained K value resulting from the first modeled problem was compared against the expected closed-form solution of

$$K = \sigma\sqrt{\pi a} \tag{5}$$

where σ is the applied stress and a is half the crack length. The numerical K value obtained from the finite element model was within 0.2% of the theoretical value. This ensured that the element size used in the finite element models is appropriate.

The second problem was adapted from (Mahmoud and Riveros 2013) where a single CFRP patch was installed over a central crack to mitigate crack propagation and reduce stress range and the normalized K was evaluated.

$$K_{norm} = \frac{K_I}{\sigma\sqrt{\pi a}} \tag{6}$$

In this case, the numerical value was compared to several other numerical studies (Chue et al. 1994; Sun et al. 1996; Naboulsi and Mall 1996), and it was concluded that the numerical result of the normalized K was within the range of other numerical studies.

The objective of this short study was to verify the 3D finite element modeling technique that will be later used in the project. Many studies have considered the single-sided and double-sided repair problems. For validation purposes, a single-sided repair benchmark problem was modeled and the results were compared against other numerical studies. The benchmark problem geometry is outlined in Figure 11, while geometrical and material properties are shown in Table 2.

3.2.1 Plate with a Center Crack

Initially, an aluminum plate with a center crack and applied normal stress was modeled prior to being repaired, as shown in Figure 12.

Figure 11. Single-sided repair plate.

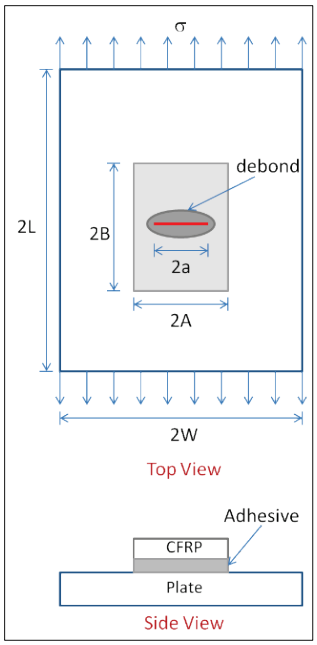

Figure 12. Plate with a center crack.

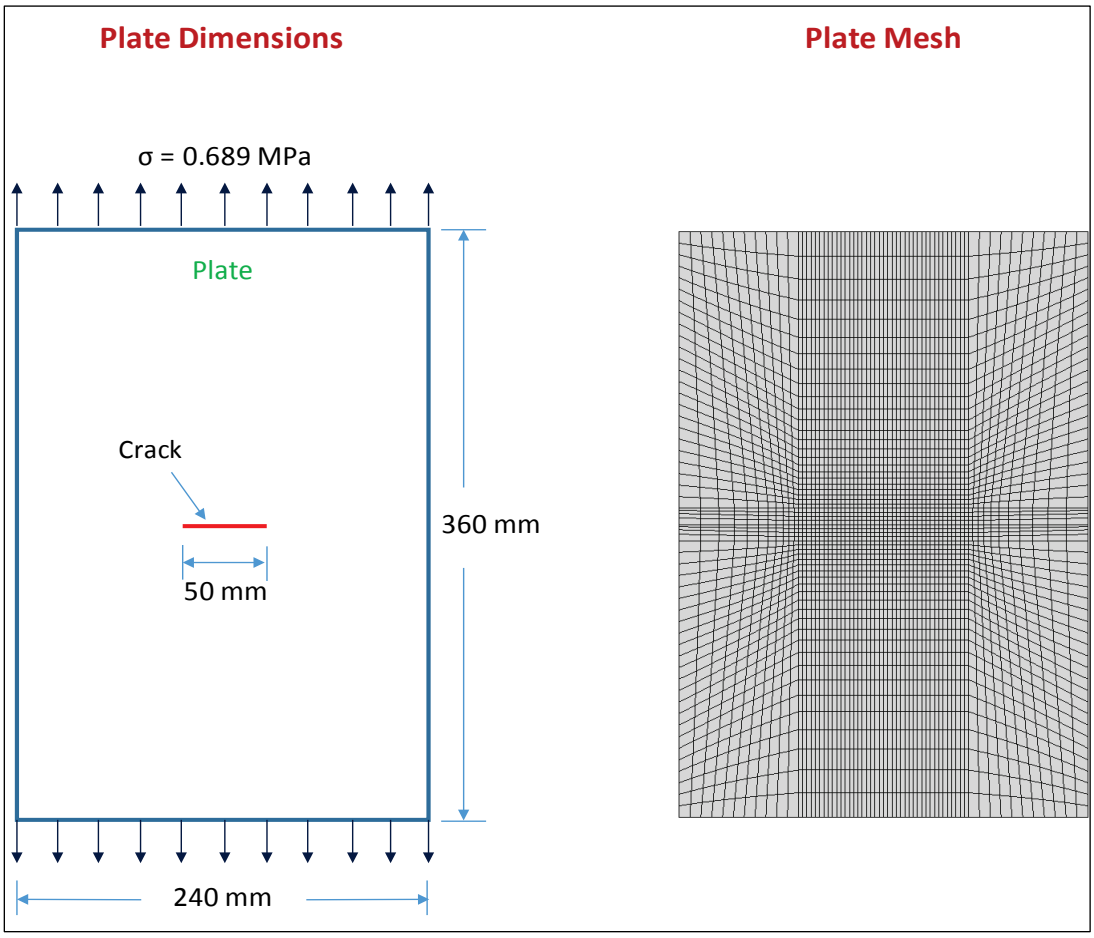

The stress intensity factor was obtained from the numerical model and compared against the value calculated using the closed-form solution. The material properties and dimensions of the plate from the single-sided repair problem (without the repair) were used in the model. The theoretical stress intensity factor (K) was calculated as:

$$K = F\sigma\sqrt{a\pi} \tag{7}$$

where F is a correction factor, σ is the applied normal stress and a is half the crack length. In this problem, σ = 0.689 MPa and a = 25 mm, and therefore,

$$K_{\text{closed-form}} = 6.186 \text{ MPa}\cdot\sqrt{\text{mm}}$$

The numerical K value was obtained from ABAQUS by requesting K outputs for 5 contours. The K value was reported as the average of the values of the last 4 contours; the first K value is considered to be inaccurate, therefore, it was ignored. The corresponding K value is

$$K_{numerical} = 6.196 \text{ MPa}\cdot\sqrt{\text{mm}}.$$

Once the numerical method was validated against a plate with a central crack, the model was modified by applying the adhesive and CFRP to mimic the simulation of a CFRP-repaired plate.

3.2.2 Single-Sided Repair

The plate, adhesive, and composite patch were all modeled as solid elements with material properties from Table 2. Contact formulation between the three different layers was implemented, including some debonding effect at the crack vicinity. The K value was requested using 5 contours, and the final K value was computed similar to the case of the plate with a central crack without repairs. The value from contour 1 was ignored, while the average value from the next 4 contours was used to obtain the K value of the repaired plate. In previous numerical studies, a normalized K value was calculated as follows:

$$K = \frac{K_I}{\sigma\sqrt{a\pi}} \tag{8}$$

Resulting values from previous studies are presented in Table 3. While the previous studies included biaxial stress, only the uniaxial stress case was modeled in this case (λ=0). The second row in Table 3 represents the relevant results to which the numerical results of the single-sided repair problem are compared to from previous numerical studies. The resulting K_{num} = 3.322 MPa·$\sqrt{mm}$, therefore, the normalized K = 0.537, falls in the range of previous results. An overview of the plate dimensions and mesh are shown in Figure 13.

Table 3. Normalized stress intensity factor K at the mid-plane for a single-sided repair (Mahmoud and Riveros 2013).

λ	Chue et al. (1994) Three-dimensional	Sun et al. (1996) Two-dimensional	Sun et al. (1996) Three-dimensional	Naboulsi and Mall (1996) Three layer model Two-dimensional
-2	0.392	0.493	0.565	0.552
0	0.481	0.536	0.612	0.570
+2	0.571	0.579	0.660	0.609

Figure 13. Overview of the finite element model used.

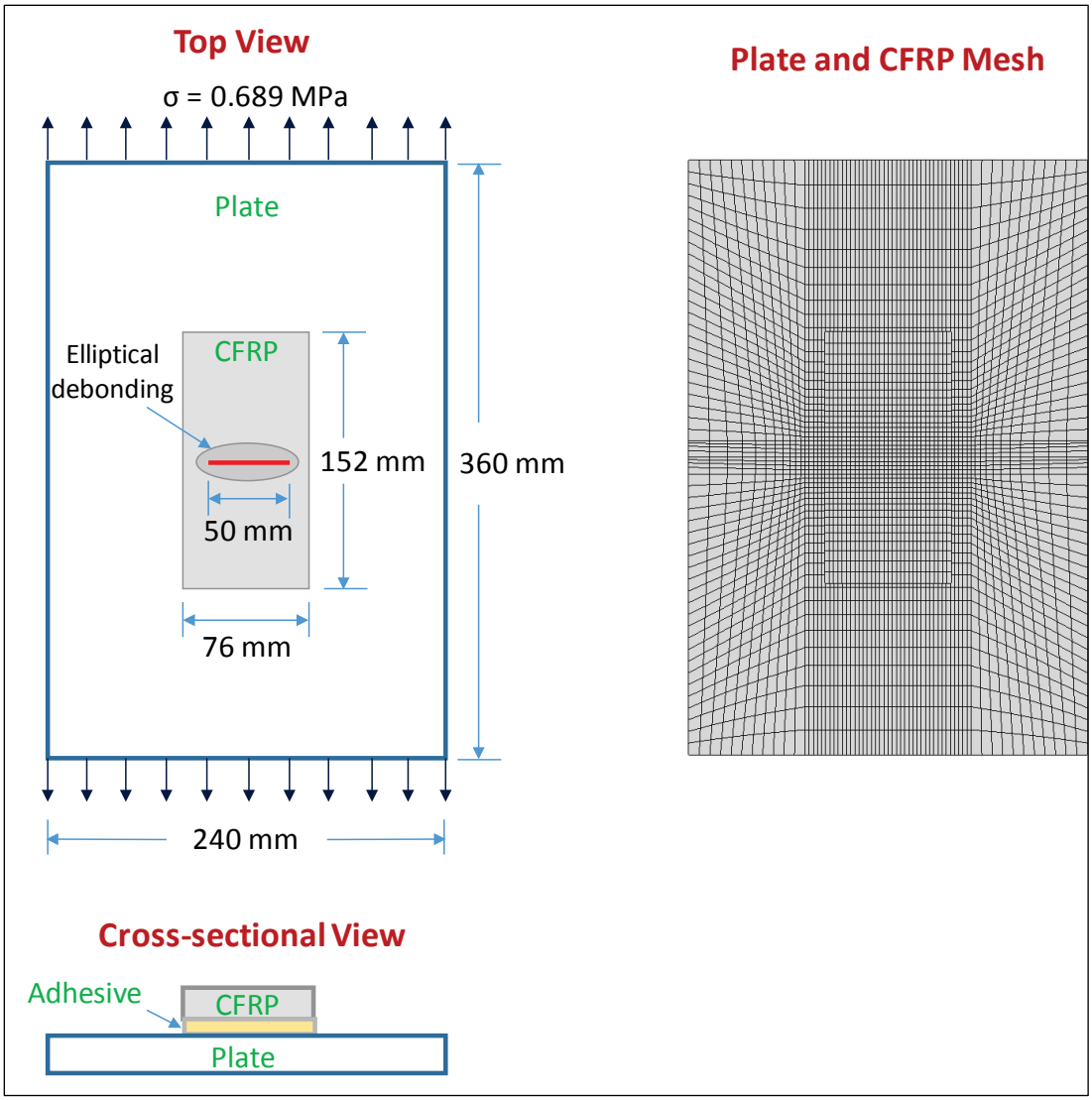

4 Results and Discussion

A parametric study was conducted to determine the effects of several CFRP repair schemes on mitigating crack propagation in steel panels under loading and boundary conditions that are representative to what may be experiences by a miter gate. A typical finite element model used in the simulations is shown in Figure 14 and a typical plate/CFRP mesh is shown in Figure 15. The figure shows the retrofitted steel panel, the CFRP patch, and the volume of water used in the simulation. It is worth noting that the water level was set to be slightly higher than that of the CFRP. This is because setting the water at the same height as that of the CFRP resulted in numerical instability. The varied parameters that were considered in the study included the crack length, stage of gate operation, single-sided CFRP repairs, double-sided CFRP repairs, and repairs with prestressed CFRP patches. The study included five different crack lengths and four different gate angles at different stages of operation. A varying angle of initial water velocity was implemented to simulate the gate at four different stages of operation (from open to close). A total of forty-five models were analyzed, twenty of which contained single-sided CFRP patches, twenty contained double-sided CFRP patches, and 5 of which did not include single patch CFRP repairs, as outlined in Table 4. The water velocity normal to the plate was set to 10.67 mm/sec using linear distribution.

Figure 14. Overview of the finite element model used.

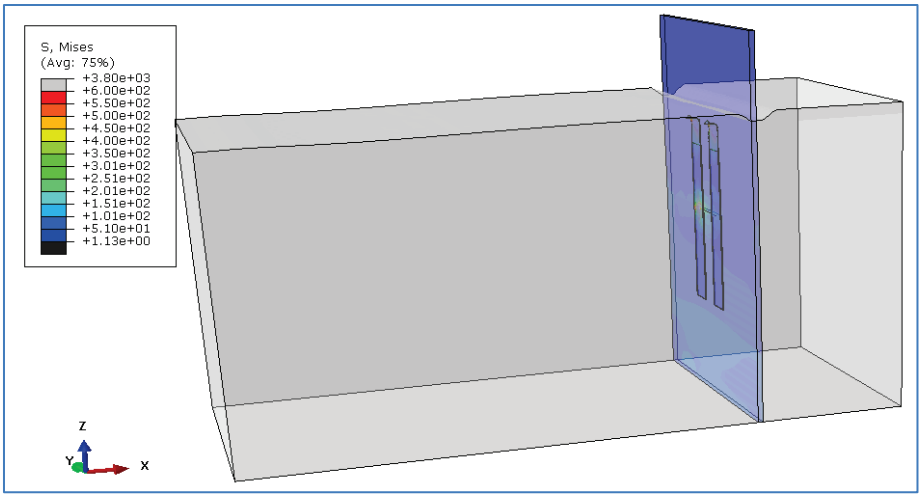

Figure 15. Plate/CFRP mesh.

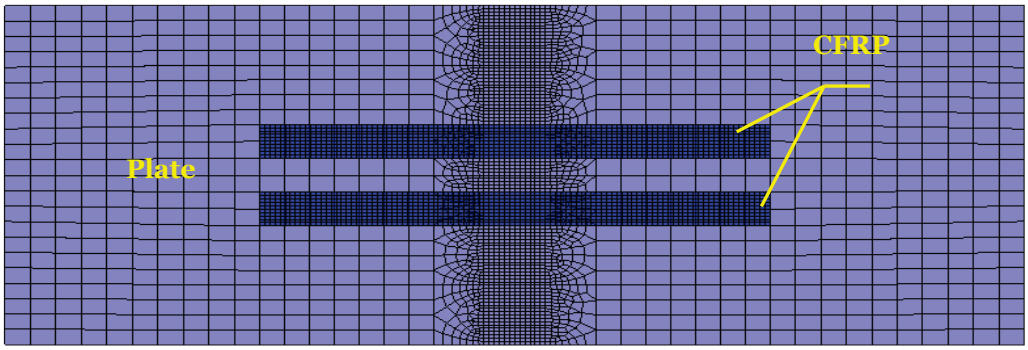

Table 4. Analysis Matrix.

							No. of Models
Single-sided CFRP Patch	Crack Length (mm)	25	50	75	100	125	5 x 4
	Horizontal Velocity Angle	0°	30°	60°	88°	NA	
Double-sided CFRP Patch	Crack Length (mm)	25	50	75	100	125	5 x 4
	Horizontal Velocity Angle	0°	30°	60°	88°	NA	
No CFRP	Crack Length (mm)	25	50	75	100	125	5
						Total number of Models	45

4.1 Contour Results

From the computational fluid dynamics (CFD) analysis, deflection and normal stress contours were plotted for closed and opened gate positions. The observed displacement (mm) contour in Figure 16(a) validates the expected pattern. For the closed case, the deflection is at its maximum at ¾ of plate height since the maximum water velocity is at the same location. Moreover, the deflection is uniform across the width of plate as a result of the pinned boundary condition at the restraint out of plane at the top two corners. When the gate is in an open position, the gate is restrained only on the left side (pin at the bottom, roller at the top corner) and the water impacts the gate at ¾ of gate height and allowed to flow around the free edge of the gate. In this case, the anticipated maximum deflection would be at the top right portion of the gate, as illustrated in Figure 16(b). Normal stress (MPa) contours are presented in Figure 17. Given symmetric boundary conditions, the normal stress distribution when a gate is closed under gravity and water loads match the expected normal stress distribution, as illustrated in Figure 17(a). Similarly, because of the load and boundary conditions used, a diagonal normal stress distribution is

anticipated for an open gate, with high stresses around the pinned and roller connections, as shown in Figure 17(b). It is important to note that the high stress concentration area at the bottom left corner is known to be a problematic region with cracks developing in the pintle.

Figure 16. Deflection contours for (a) closed and (b) open gate.

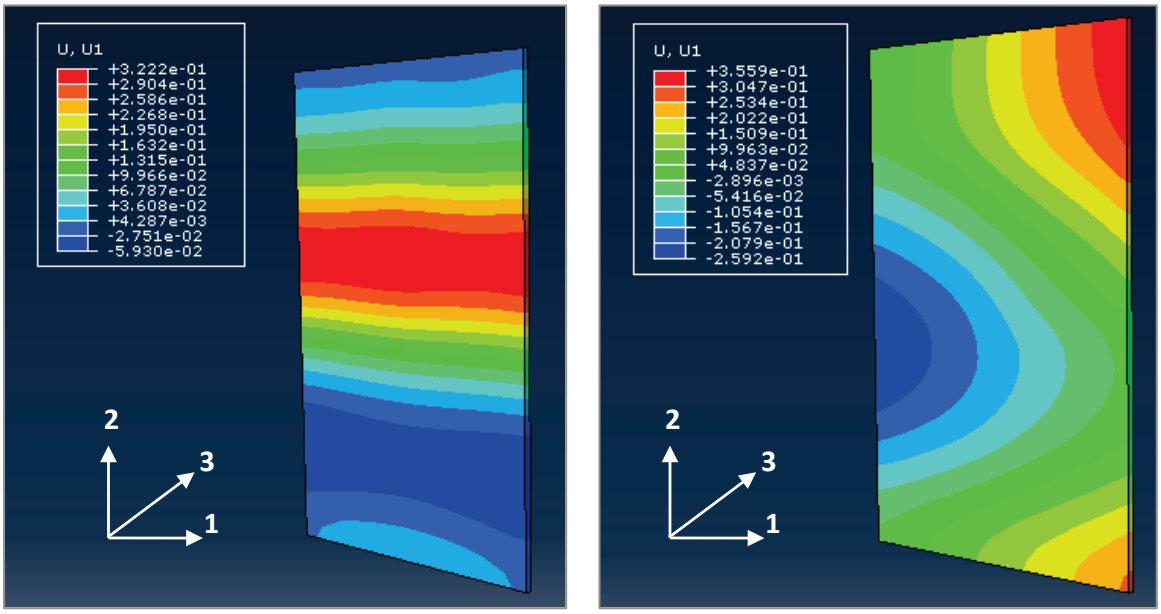

(a) (b)

Figure 17. Normal stress contours for (a) closed and (b) open gate.

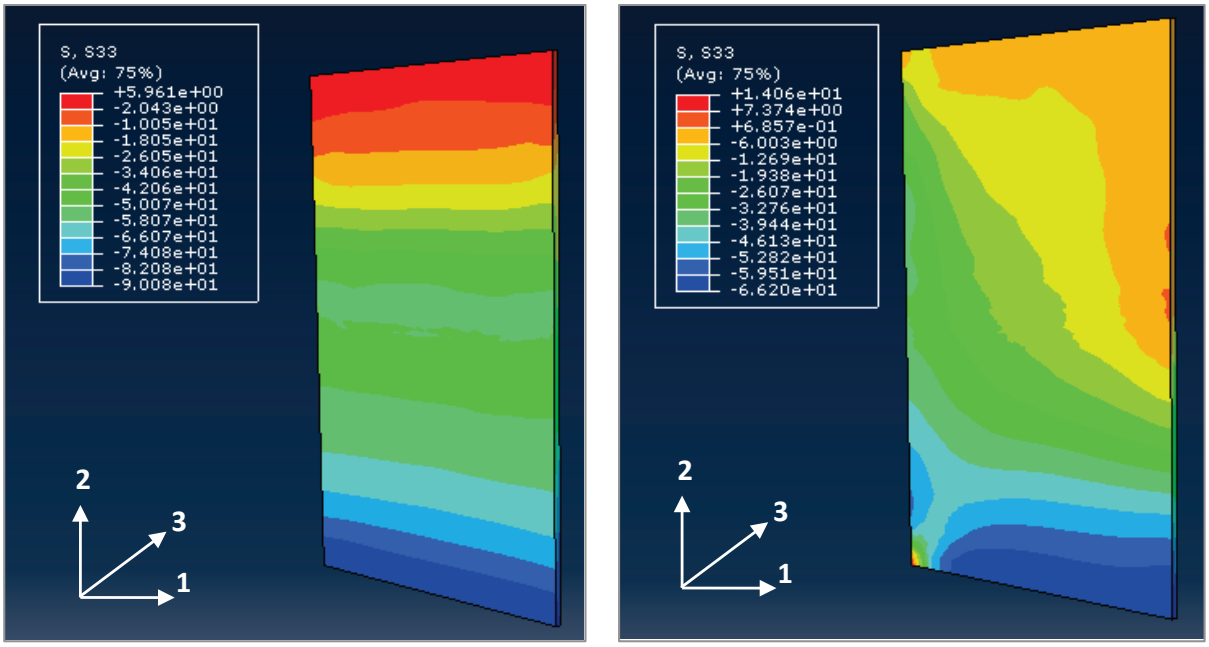

(a) (b)

In addition to plate contours, stress contours were obtained for the CFRP patches at different crack lengths, as shown in Figure 18. While the CFRP stresses are concentrated around the crack, the distribution is fairly similar when the crack length is under the CFRP patch. However, as the crack propagates beyond the CFRP, there is a more noticeable stress concentration at the crack location on the CFRP patches. Similarly, Figure 19 shows the von Mises stress contours for the CFRP and the plate for the top side of the plate and Figure 20 shows the von Mises stresses for the plate on the backside of the plate.

Figure 18. CFRP stress contours for different crack length.

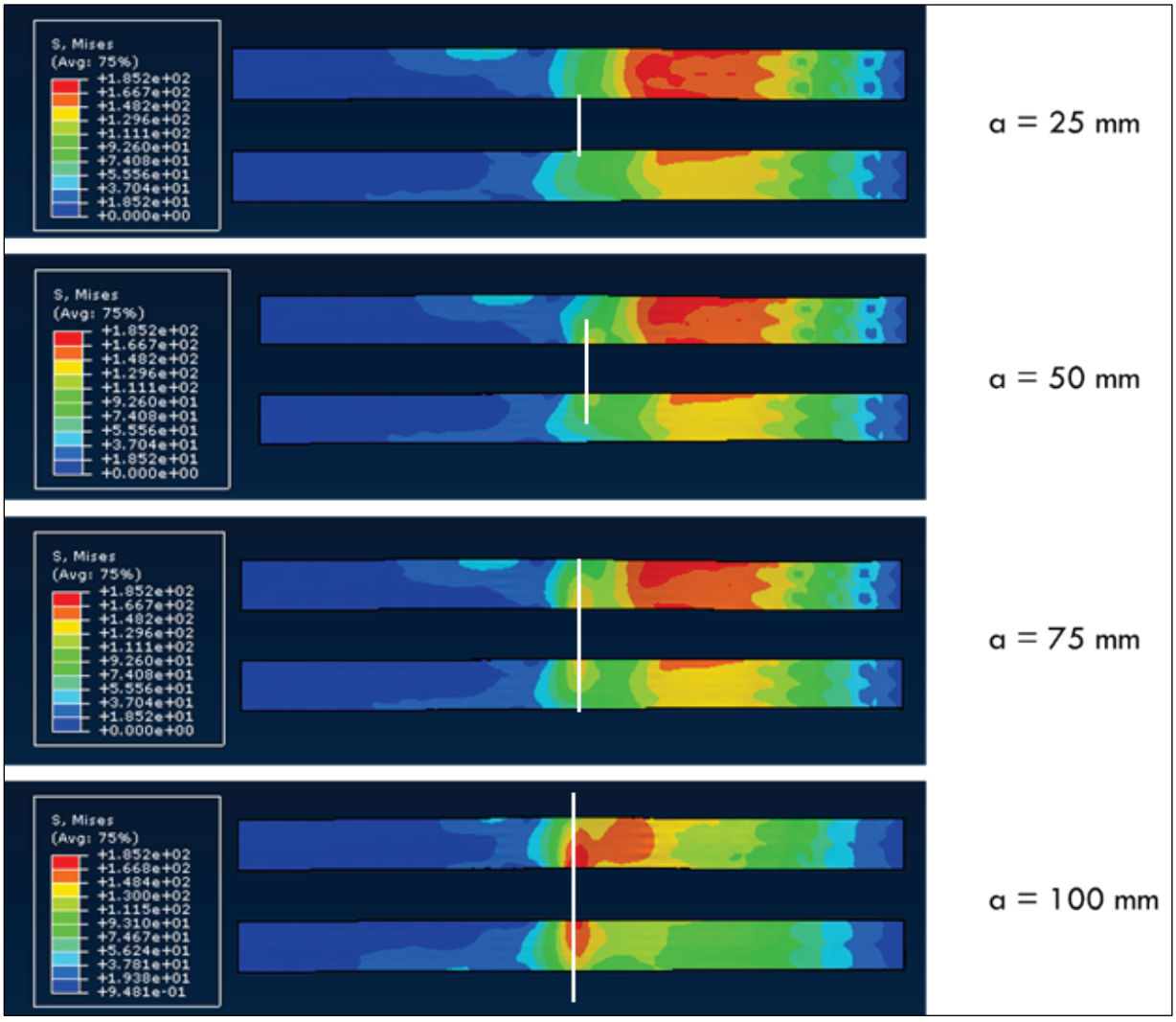

Figure 19. CFRP/plate stress contours for a crack directly beneath the CFRP.

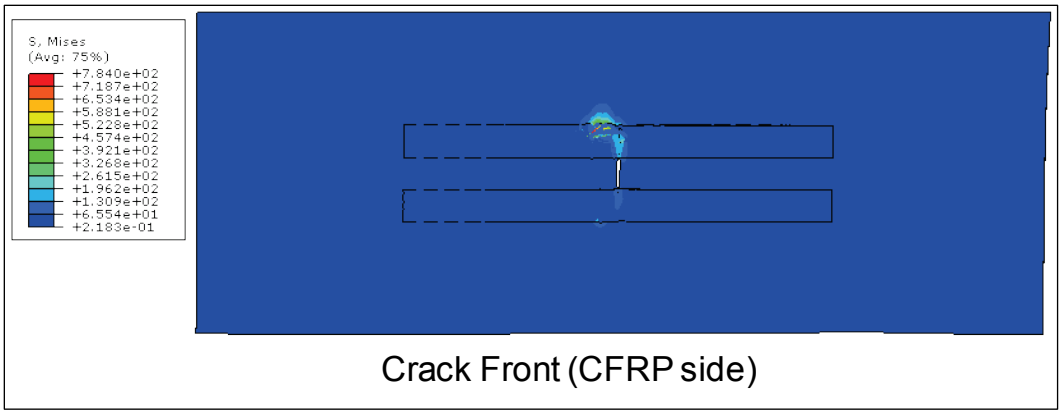

Figure 20. Plate stress contours for a crack directly beneath the CFRP.

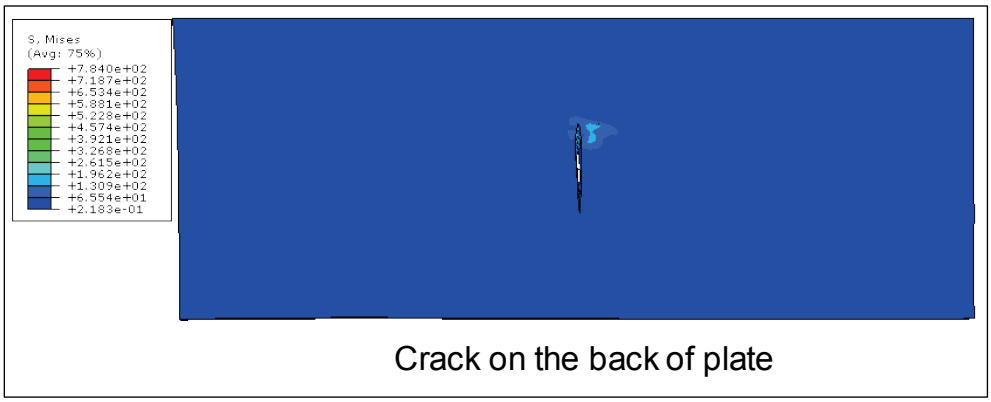

4.2 Half crack length vs. Number of Cycles for CFRP-repaired steel plates using C = $2.4 \cdot 10^{-12}$

Based on the obtained numerical *K* values and Paris' Law, the number of cycles (*N*) was calculated for a given half crack length (a) for all 45 models. Two main parameters were considered when analyzing the results: single- vs. double-sided CFRP repair, prestressed vs. nonprestressed CFRP repair, and combinations of the two (i.e., single-sided prestressed CFRP vs. double-sided prestressed CFRP). Figure 21 shows *a* versus *N* for a plate repaired with single-sided CFRP patches, when water velocity changes direction from perpendicular to almost parallel to the plate. For the most critical case, when the water is perpendicular to the plate (angle is 0^{o}), it can be observed that the CFRP has a clear impact on the increase of the number of cycles (a 1.63 times increase in life). Though previous studies have estimated an improvement of fatigue life of about 3 times, a smaller CFRP effect is expected due to the fact that the Paris law constant, *C*, represents a corrosive environment condition. Previous studies referred to in-air conditions and not marine conditions. In addition, the applied loads, coupled with the

boundary conditions, results in bending in the plate that aggravates the crack opening condition on the panel side experiencing positive bending. All previous studies did not have such a condition since the panels were loaded under pure axial tension. For the cases where the water velocity angle gradually changes from 0° to 88°, the effectiveness of CFRP is shown to increase from 1.63 times improvement for 0° angle, to 2.05, 2.29, and 2.61 times improvement for 30°, 60°, and 88° angles, respectively.

Figure 21. Half crack length (*a*) vs. number of cycles (*N*) for single-sided CFRP Patch, $C = 2.4 \cdot 10^{-12}$ (mm·cycles)(MPa·√mm).

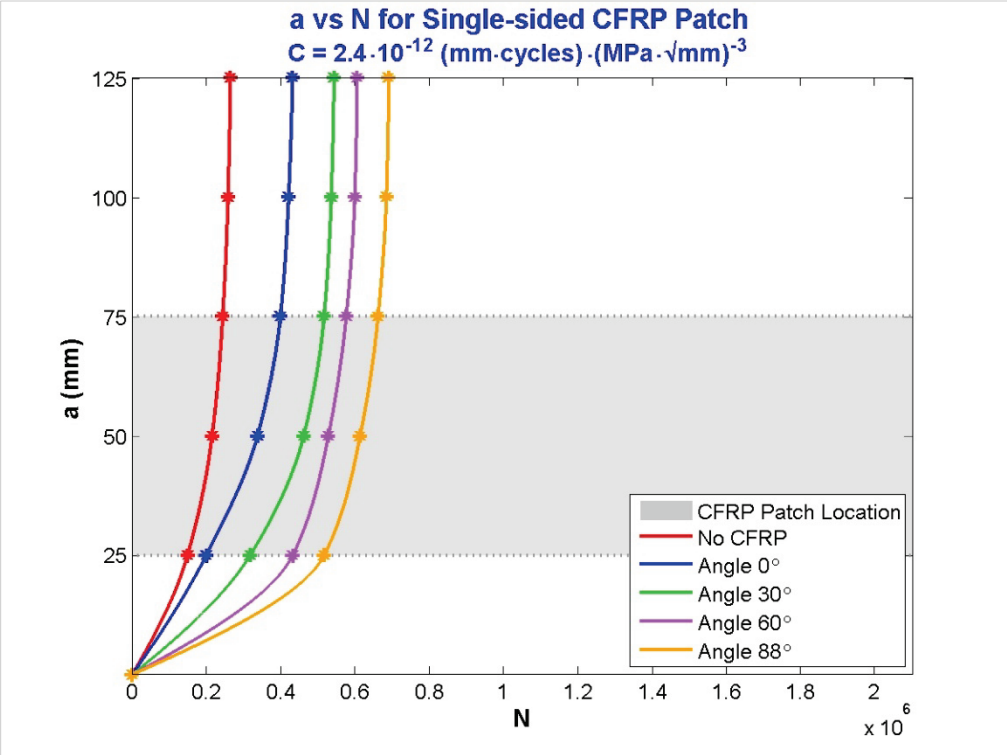

In order to evaluate the effect of prestressing on the CFRP, the CFRP patches were prestressed to a value of 500 MPa, for both single- and double-sided CFRP patches. The effect of single-sided prestressed CFRP is shown in Figure 22 with an average improvement of 26% compared to the non-prestressed CFRP case. When comparing with the unrepaired cracked plate, the observed improvements ranged from 2.05 to 3.31 times, starting from water velocity angle 0˚ to angle 88˚.

It is worth noting that although a very reasonable improvement is shown in the case of a single-sided repair, one of the reasons this repair scheme does not show drastic improvement is because a one-sided repair, particularly when prestressed, adds significant stresses to the plate

through introducing a non-centroid applied compressive axial load, which although contributing to crack closing, it introduces an applied moment that opens the crack on the unrepaired face. As shown below, the two-sided repair eliminates such conditions and results in a much higher improvement in fatigue life.

Figure 22. Half crack length (*a*) vs. number of cycles (*N*) for single-sided prestressed CFRP Patch, $C = 2.4 \cdot 10^{-12}$ (mm-cycles) (MPa-√mm).

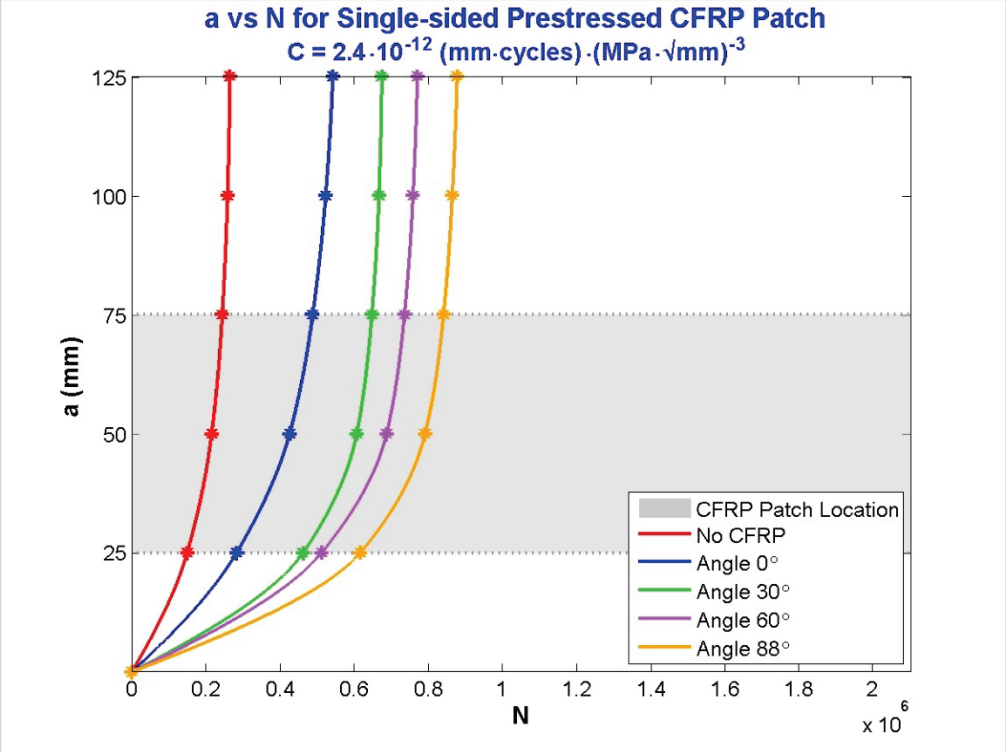

As mentioned above, the double-sided CFRP patch repair resulted in significant improvement in comparison to unrepaired plates as well as single-sided CFRP repairs, for both prestressed and non-prestressed patches. As highlighted above, part of the significant increase in the number of cycles to failure, shown in Figure 23, is attributed to the elimination of some of the asymmetrical bending due to the unbalanced axial force resulting from the single-sided repairs. It is worth noting that some bending still exists in the panel due to the nature of the applied load and boundary conditions.

Compared to an unrepaired plate, the double-sided, CFRP-repaired models resulted in 4.4 to 5.4 times increase in fatigue life, for water velocity angles of 0˚ to 88˚, respectively. Double-sided, CFRP-repaired plates also demonstrated improvements of up to 2.7 and 2.2 times in comparison to single-sided CFRP and single-sided prestressed CFRP repairs, respectively.

Figure 23. Half crack length (*a*) vs. number of cycles (*N*) for double-sided CFRP patch, *C* = 2.4·10-12 (mm·cycles)(MPa·√mm).

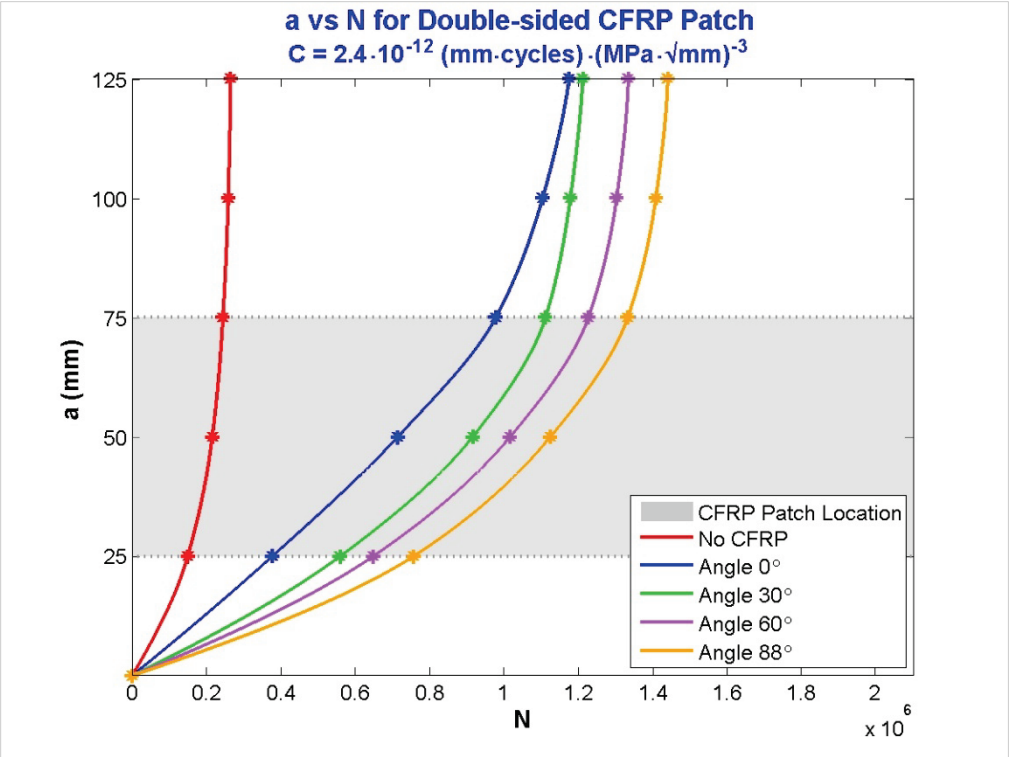

As expected, the double-sided prestressed CFRP-repaired models showed superior performance in comparison to other models. The results shown in Figure 24 demonstrated an improvement of up to 5 times that of an unrepaired model for a water velocity angle at 0°. In addition, the double-sided prestressed CFRP-repaired plate demonstrated 3.1, 2.5, and 1.14 times improvement compared to single-sided, single-sided prestressed and double-sided CFRP repairs, respectively.

Comparisons between different CFRP repairs are summarized in Table 5 in terms of ratios of improvement. In addition, Figures 25, 26, 27, and 28 show the normalized number of fatigue cycles for various crack lengths for the 0°, 30°,60, and 88° angles. The table and figures clearly show significant improvement for the double-sided CFRP patch repair cases. Furthermore, this repair method provides significant improvements over any other repair methods, particularly for longer cracks.

Figure 24. Half crack length (*a*) vs. number of cycles (*N*) for double-sided prestressed CFRP patch, *C* = 2.4·10-12 (mm·cycles)(MPa·√mm).

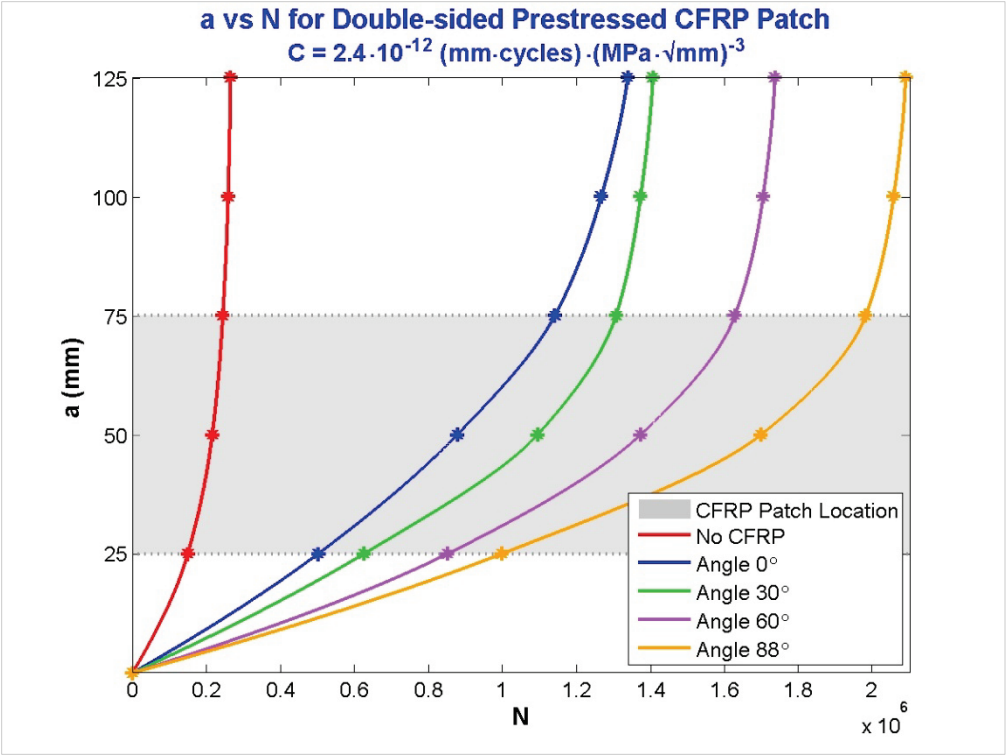

Table 5. Results Summary.

Improvements of repaired plates compared to no CFRP	Water Velocity Angle			
	0˚	30˚	60˚	88˚
Single-sided	1.63	2.05	2.29	2.61
Prestressed Single-sided	2.05	2.54	2.91	3.31
Double-sided	4.43	4.57	5.03	5.43
Prestressed Double-sided	5.05	5.31	6.55	7.88
Improvement Comparisons between different CFRP repairs				
Double-sided vs. Single-sided	2.72	2.23	2.20	2.08
Prestressed Single-sided vs. Single-sided	1.26	1.24	1.27	1.27
Prestressed Double-sided vs. Double-sided	1.14	1.16	1.30	1.45
Double-sided vs. Prestressed Single-sided	2.17	1.80	1.73	1.64
Prestressed Double-sided vs. Single-sided	3.10	2.59	2.86	3.02
Prestressed Double-sided vs. Prestressed Single-sided	2.47	2.09	2.25	2.38

Figure 25. Number of cycles vs. half crack length normalized to the case of no CFRP for an angle of 0°.

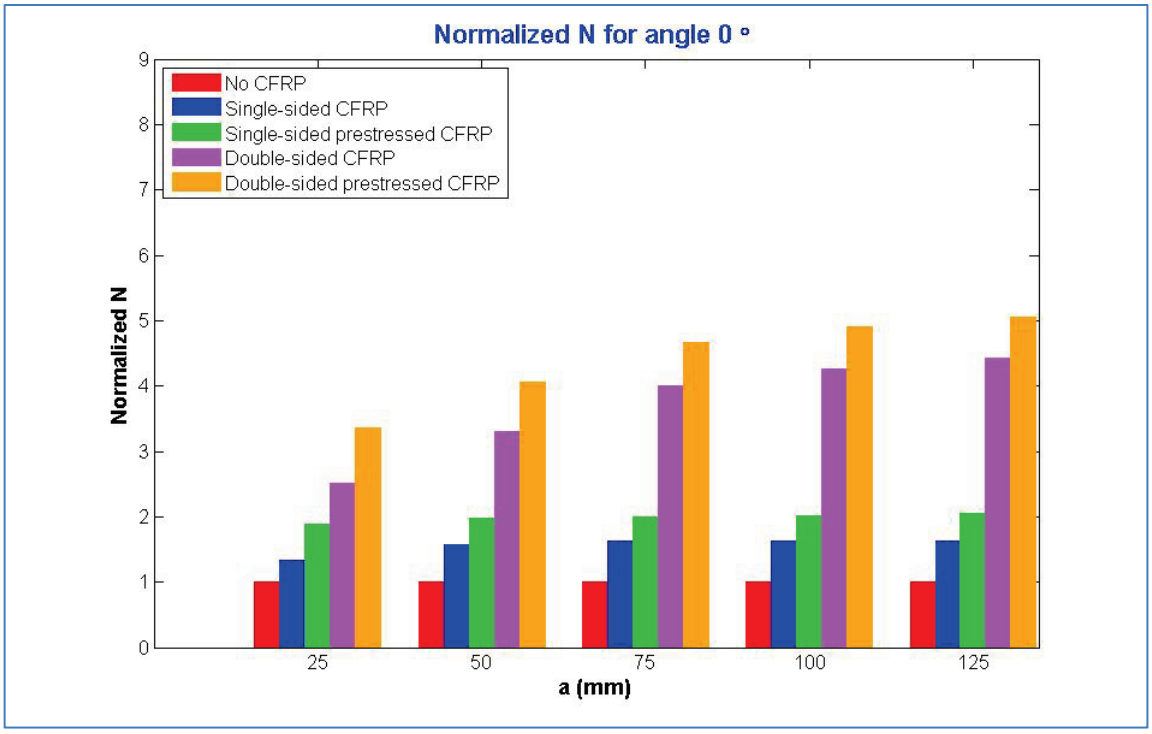

Figure 26. Number of cycles vs. half crack length normalized to the case of no CFRP for an angle of 30°.

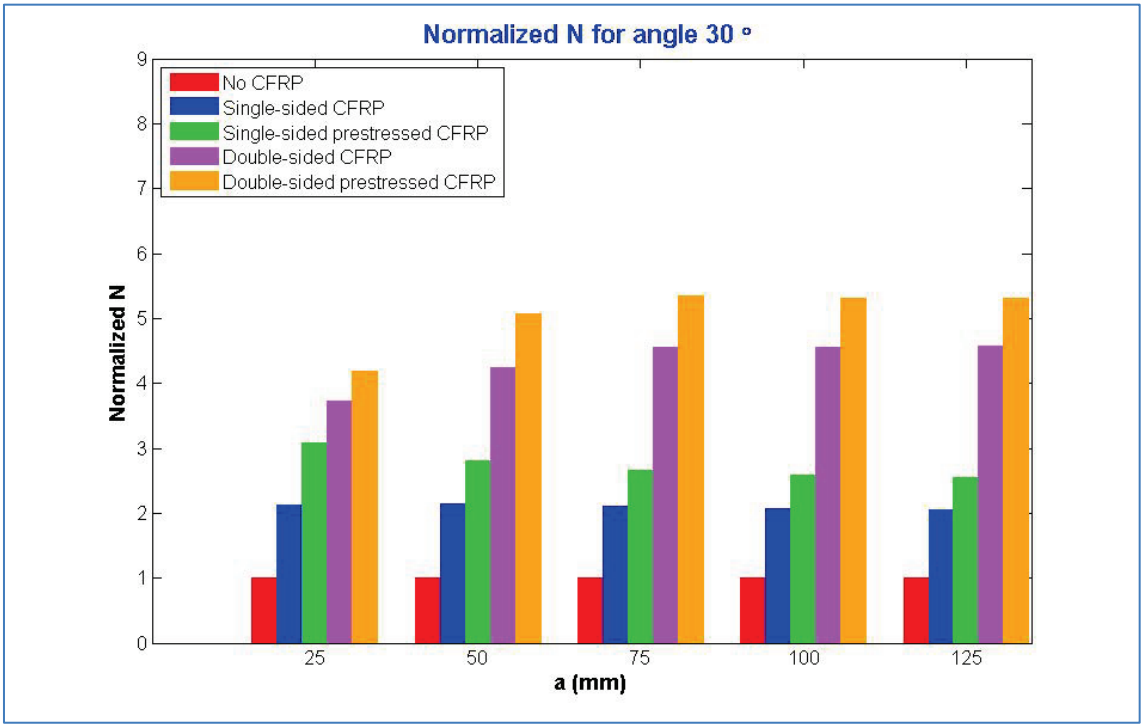

Figure 27. Number of cycles vs. half crack length normalized to the case of no CFRP for an angle of 60°.

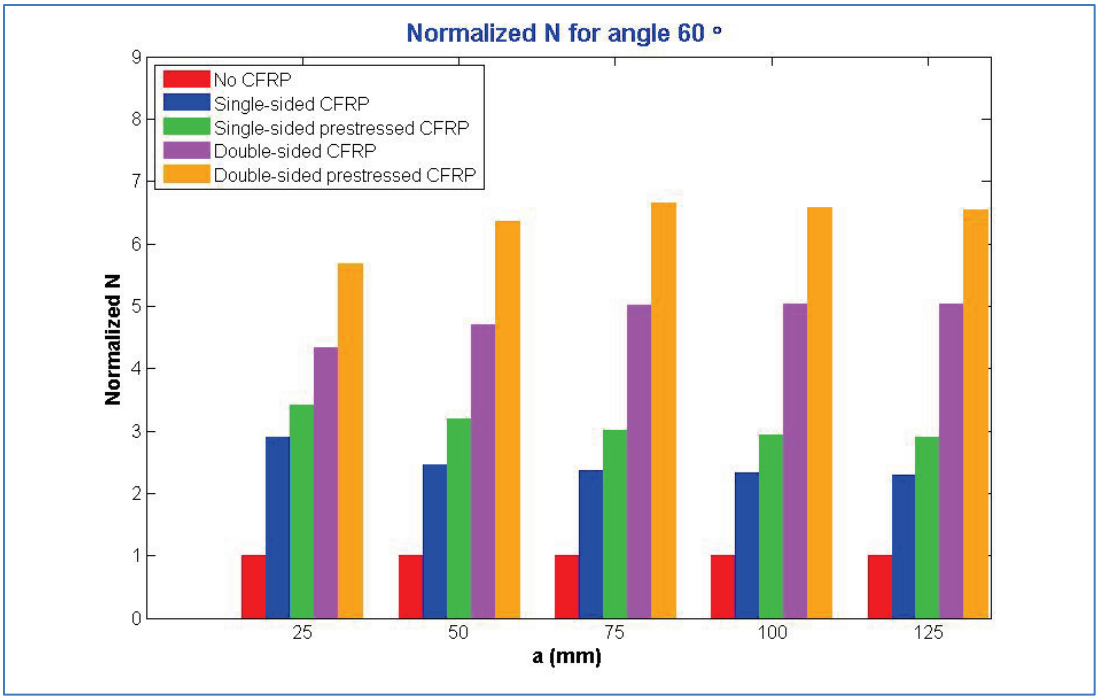

Figure 28. Number of cycles vs. half crack length normalized to the case of no CFRP for an angle of 88°.

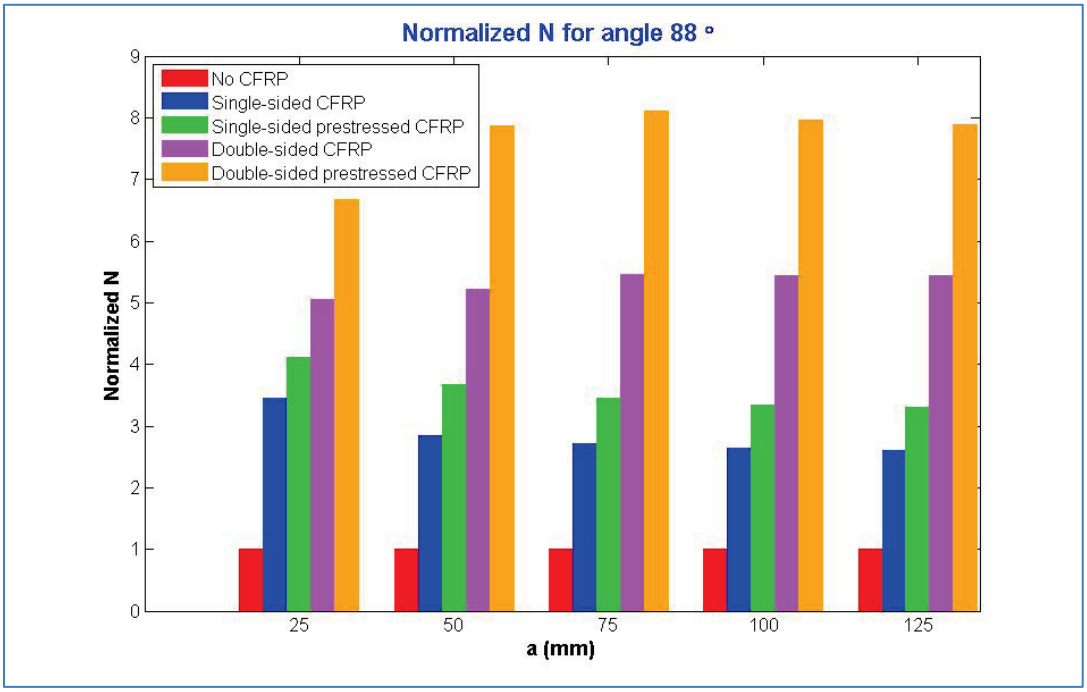

4.3 Half crack length vs. Number of Cycles for CFRP-repaired steel plates using C = 5.21·10^{-13}

The C parameter equal to 2.4·10^{-12} (mm·cycles)·(MPa·$\sqrt{mm}$) corresponds to corroded conditions. The crack propagation analysis was repeated for uncorroded conditions, C=5.12·10^{-13} (mm·cycles)·(MPa·$\sqrt{mm}$), to represent the condition of uncorroded gate. This will bound the solution so that an assessment can be made between the best and worst possible improvement. The C value of 5.12·10^{-13} (mm·cycles)·(MPa·$\sqrt{mm}$) was chosen in accordance with British Standards (BS) 7910 (2012). The graphs for half crack length (a) vs. number of cycles (N) were generated to quantify the differences between corroded and uncorroded cases. Individual results, similar to the previous section, for single-sided CFRP, single-sided prestressed CFRP, double-sided CFRP, and double-sided prestressed CFRP are shown in Figures 29 - 32, respectively. Comparisons between the different CFRP repairs for C = 5.12·10^{-13} (mm·cycles)·(MPa·$\sqrt{mm}$) yield the same results and conclusions, as expected. However, it is clear that N increases significantly for each case in each plot for the two different C values. More specifically, the difference is shown in Figure 33, where a vs. N is plotted for the double-sided prestressed CFRP repair for both C values. For each water velocity angle curve, the N values for an uncorroded steel plate are approximately 4.6 times higher than the respective N values for the corroded conditions.

Figure 29. Half crack length (a) vs. number of cycles (N) for single-sided CFRP patch, C = 5.21·10^{-13} (mm·cycles)(MPa·√mm).

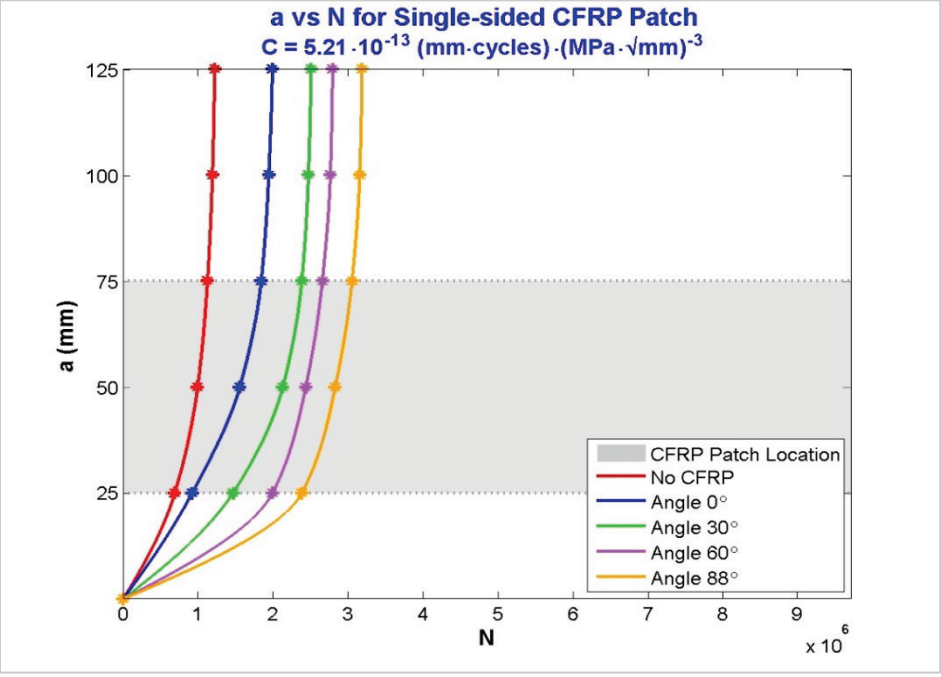

Figure 30. Half crack length (*a*) vs. number of cycles (*N*) for single-sided prestressed CFRP patch, $C = 5.21 \cdot 10^{-13}$ (mm·cycles)(MPa·√mm).

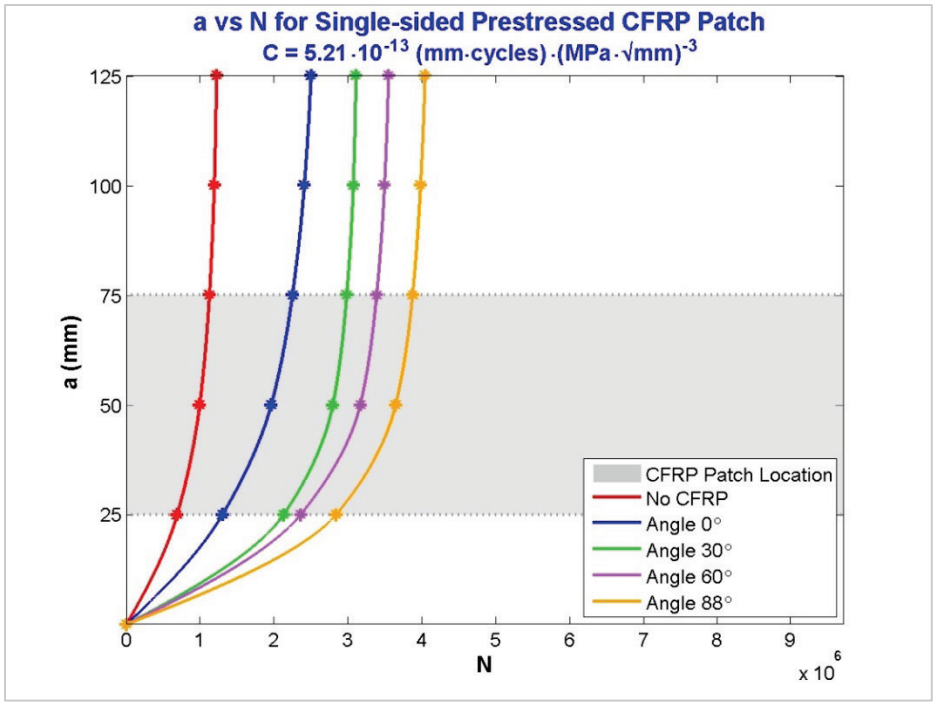

Figure 31. Half crack length (a) vs. number of cycles (*N*) for double-sided CFRP patch, $C = 5.21 \cdot 10^{-13}$ (mm·cycles)(MPa·√mm).

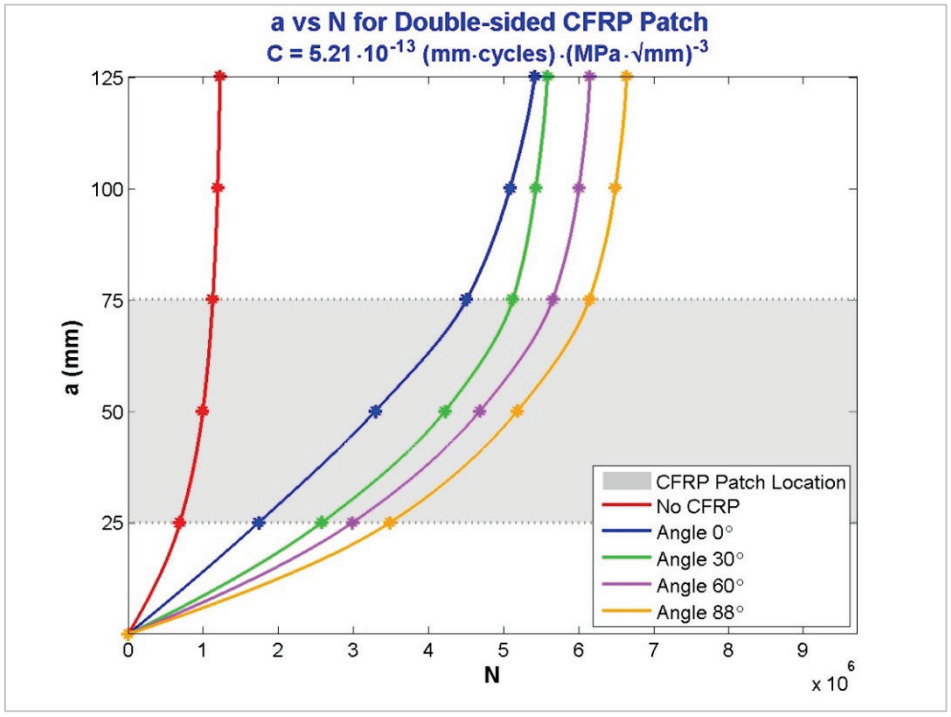

Figure 32. Half crack length (*a*) vs. number of cycles (*N*) for double-sided prestressed CFRP patch, $C = 5.21 \cdot 10^{-13}$ (mm·cycles)(MPa·√mm).

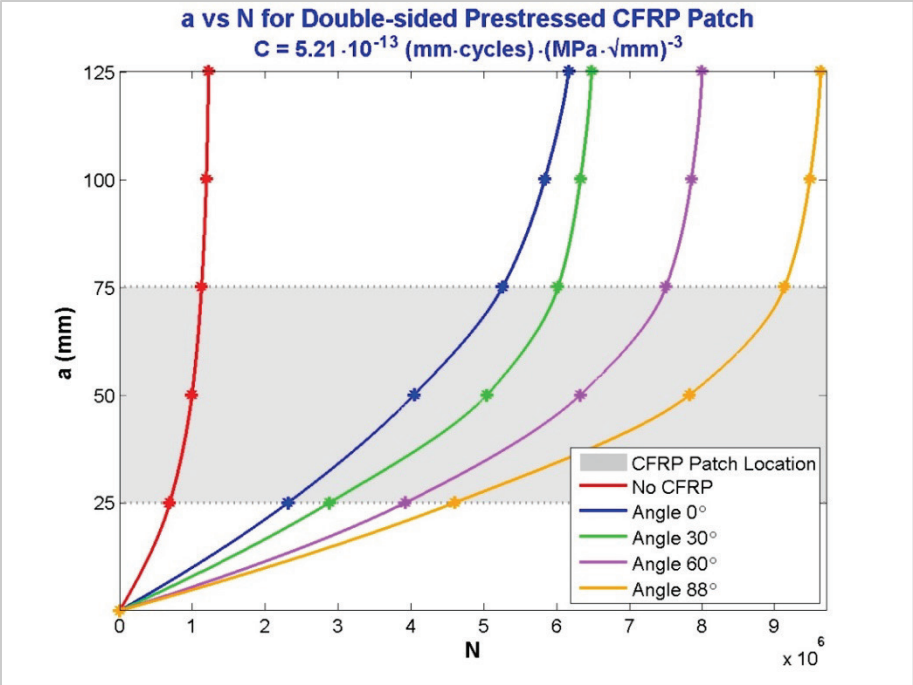

Figure 33. Half crack length (*a*) vs. number of cycles (*N*) for double-sided prestressed CFRP patch.

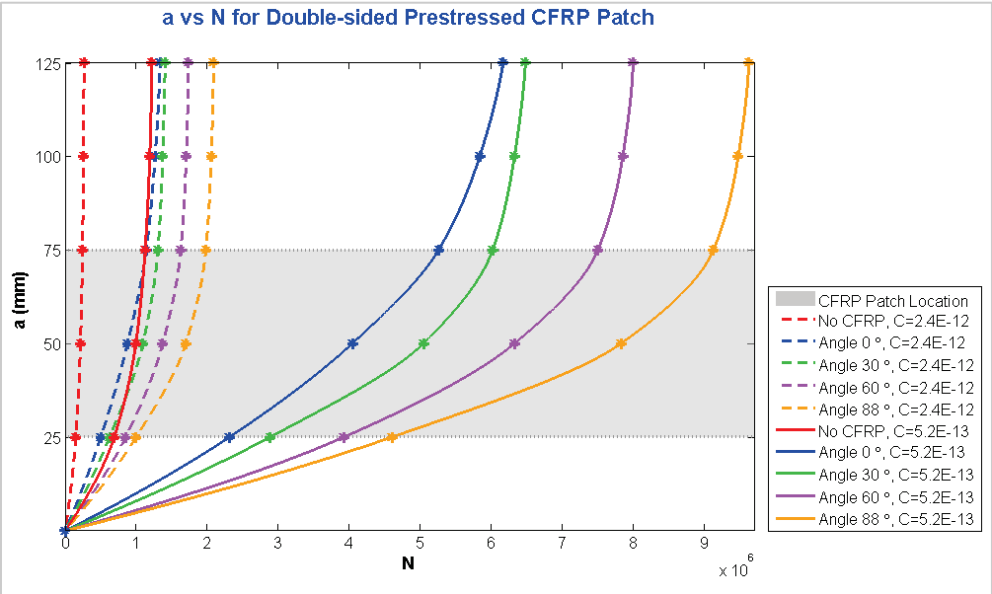

4.4 $\Delta K_{eff}/\Delta K_{thresh}$ vs. a with C = $2.4 \cdot 10^{-12}$

In addition to *a* vs. *N*, $\Delta K_{eff}/\Delta K_{threshold}$ vs. *a*, results were also plotted, where $\Delta K_{threshold}$ refers to the threshold stress intensity factor value above which the crack starts to propagate. For steel, $\Delta K_{threshold}$ can be assumed as

3 ksi$\sqrt{\text{in.}}$ = 104 MPa$\sqrt{\text{mm}}$. Figure 34 shows this plot for different velocity angles for both unrepaired and single-sided repaired plates. A $\Delta K_{eff}/\Delta K_{threshold}$ ratio larger than one indicates that the crack is propagating. Additionally, the effectiveness of the CFRP is clear, since the slope of the plotted ratio as a function of crack length decreases in the region where the CFRP is applied as compared to the unrepaired plate. Furthermore, the stress intensity factor is reduced when the crack is under the CFRP, while it rapidly increases as the crack propagates beyond the CFRP patch. This is true except for the single-sided repaired and unrepaired CFRP cases as shown in Figures 34, 35, 38, and 39. In these figures, an increase in the slope is observed, particularly in the case of 60° and 88° angles, highlighting the undesired asymmetrical load effect. Moreover, crack propagation is significantly slowed down in the cases of double-sided and double-sided prestressed CFRP repairs, as shown in Figures 36, 37, 40, and 41 compared to single-sided CFRP repairs in Figures 34, 35, 38, and 39.

Figure 34. $\Delta K_{eff}/\Delta K_{threshold}$ vs. a for single-sided CFRP patch, $C = 2.4 \cdot 10^{-12}$ (mm·cycles)(MPa·√mm).

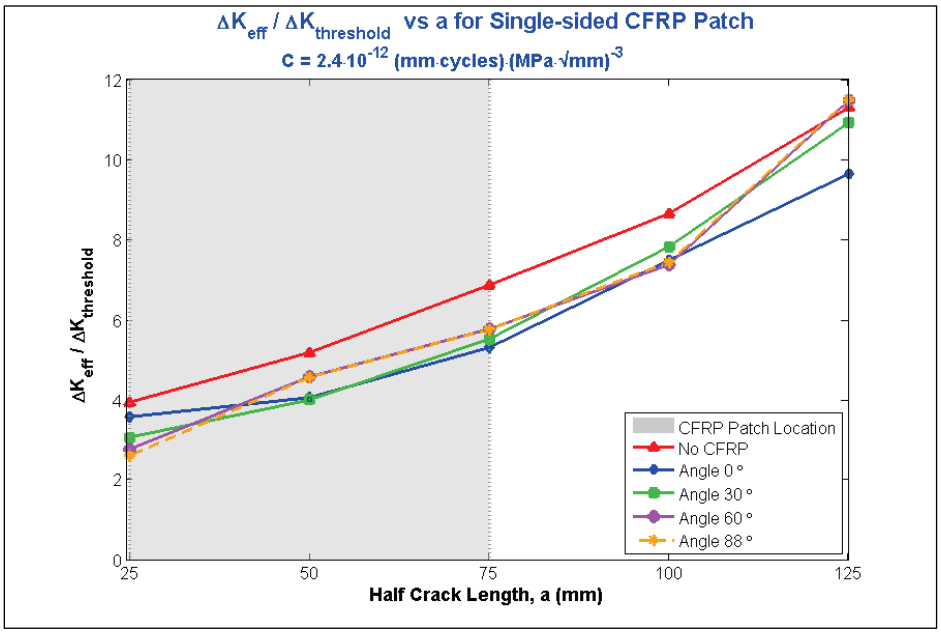

Figure 35. $\Delta K_{eff}/\Delta K_{threshold}$ vs. a for single-sided prestressed CFRP patch, $C = 2.4 \cdot 10^{-12}$ (mm·cycles)(MPa·√mm).

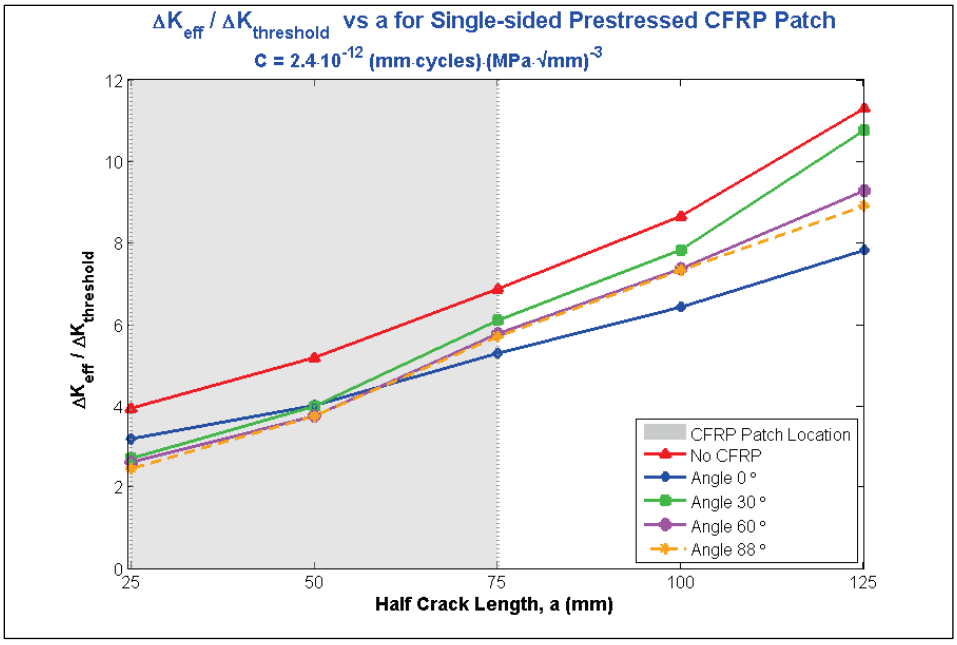

Figure 36. $\Delta K_{eff}/\Delta K_{threshold}$ vs. a for double-sided CFRP patch, $C = 2.4 \cdot 10^{-12}$ (mm·cycles)(MPa·√mm).

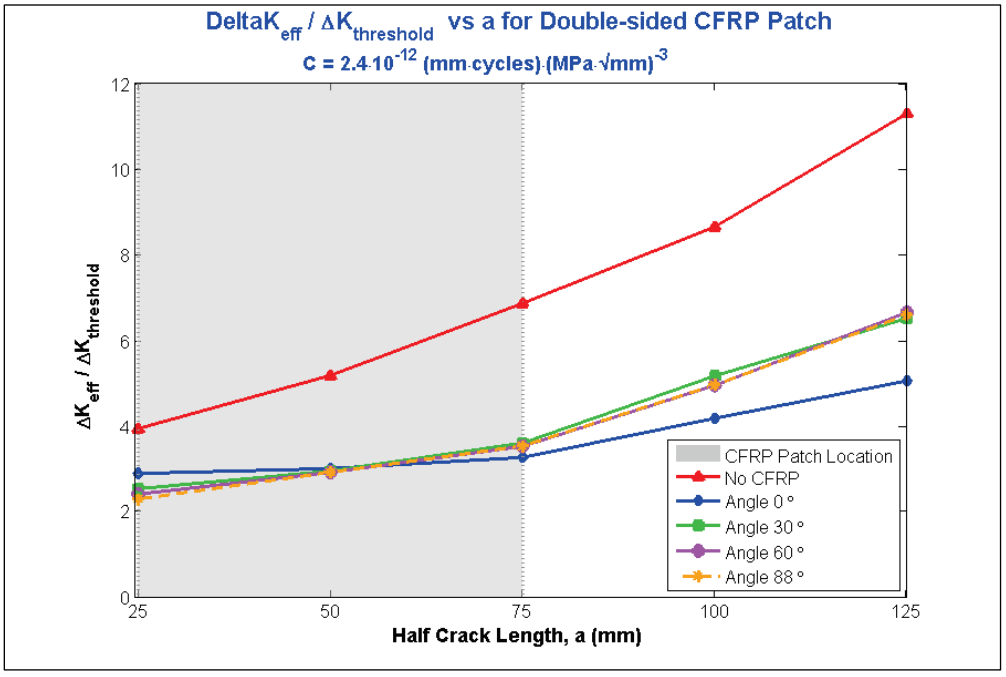

Figure 37. $\Delta K_{eff}/\Delta K_{threshold}$ vs. a for double-sided prestressed CFRP patch, $C = 2.4 \cdot 10^{-12}$ (mm·cycles)(MPa·√mm).

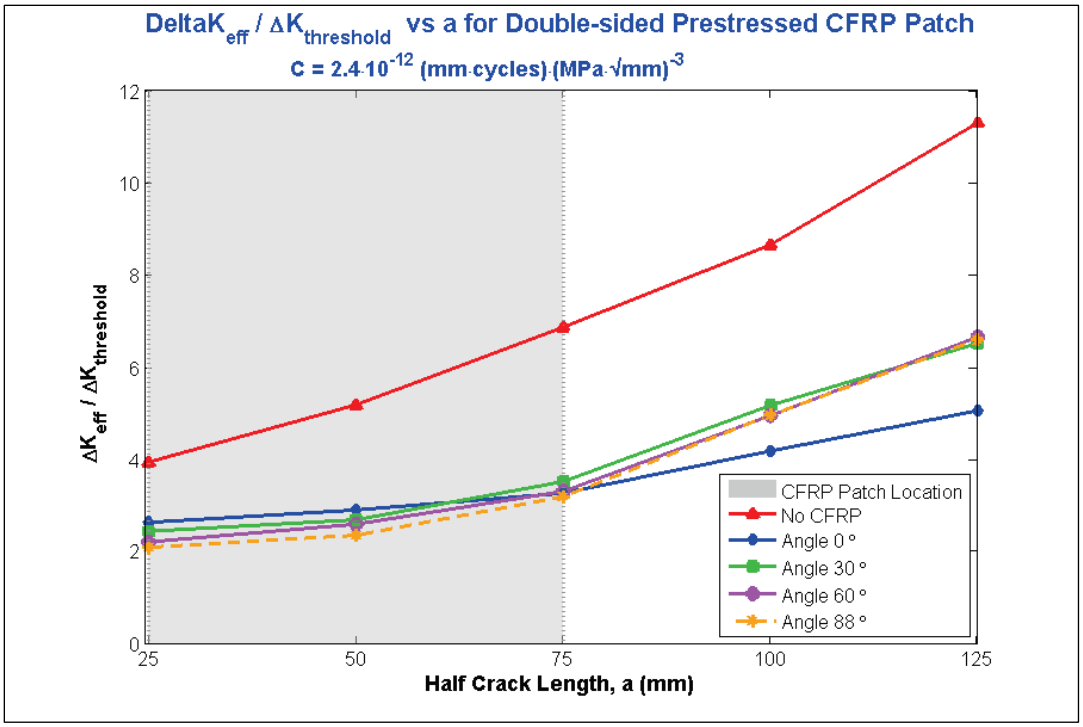

4.5 $\Delta K_{eff}/\Delta K_{thresh}$ vs. a with C = $5.21 \cdot 10^{-13}$

Figure 38. $\Delta K_{eff}/\Delta K_{threshold}$ vs. a for single-sided CFRP patch, $C = 5.21 \cdot 10^{-13}$ (mm·cycles)(MPa·√mm).

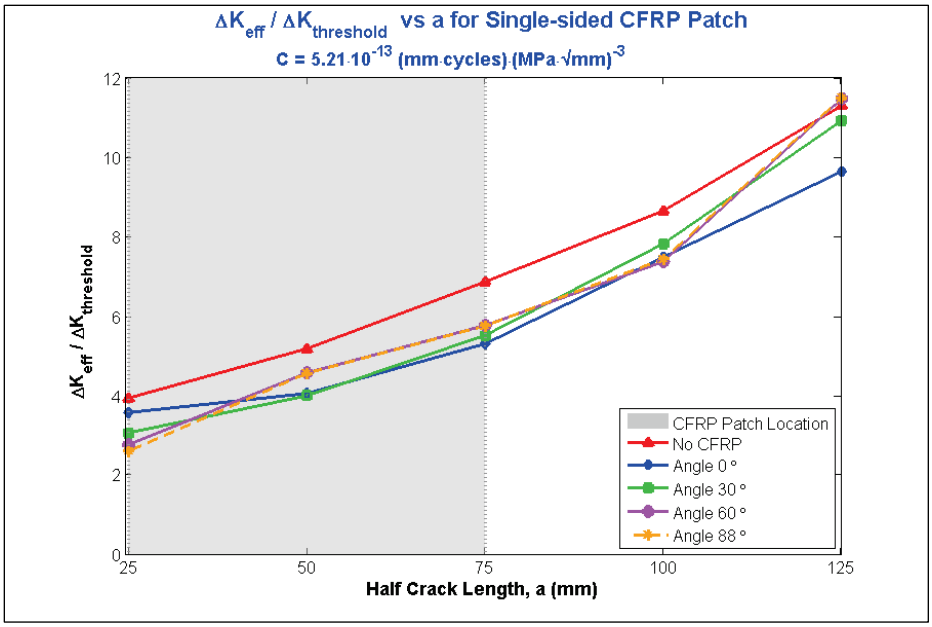

Figure 39. $\Delta K_{eff}/\Delta K_{threshold}$ vs. a for single-sided prestressed CFRP patch, $C = 5.21 \cdot 10^{-13}$ (mm-cycles)(MPa-√mm).

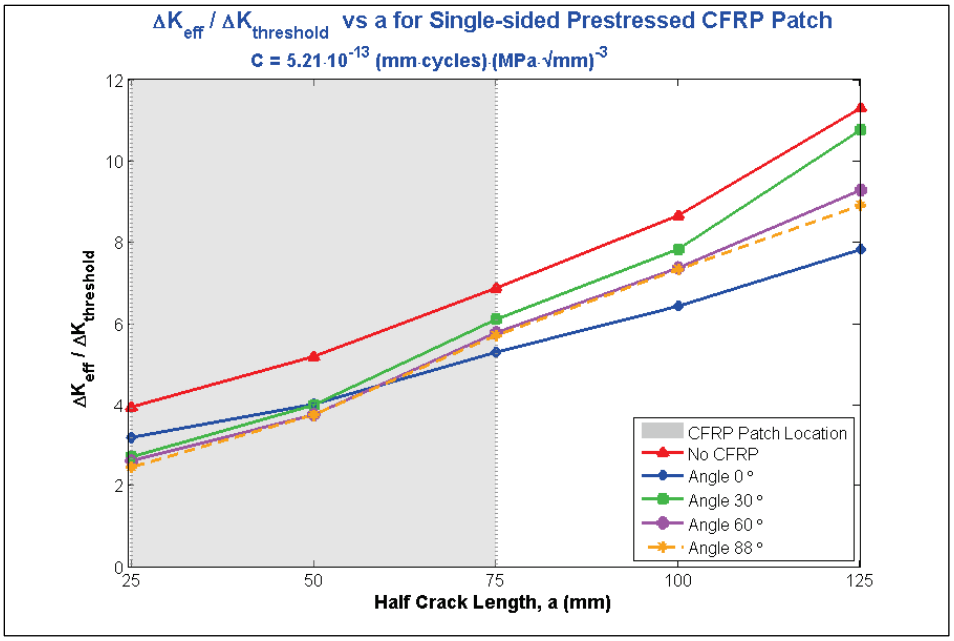

Figure 40. $\Delta K_{eff}/\Delta K_{threshold}$ vs. a for double-sided CFRP patch, $C = 5.21 \cdot 10^{-13}$ (mm-cycles)(MPa-√mm).

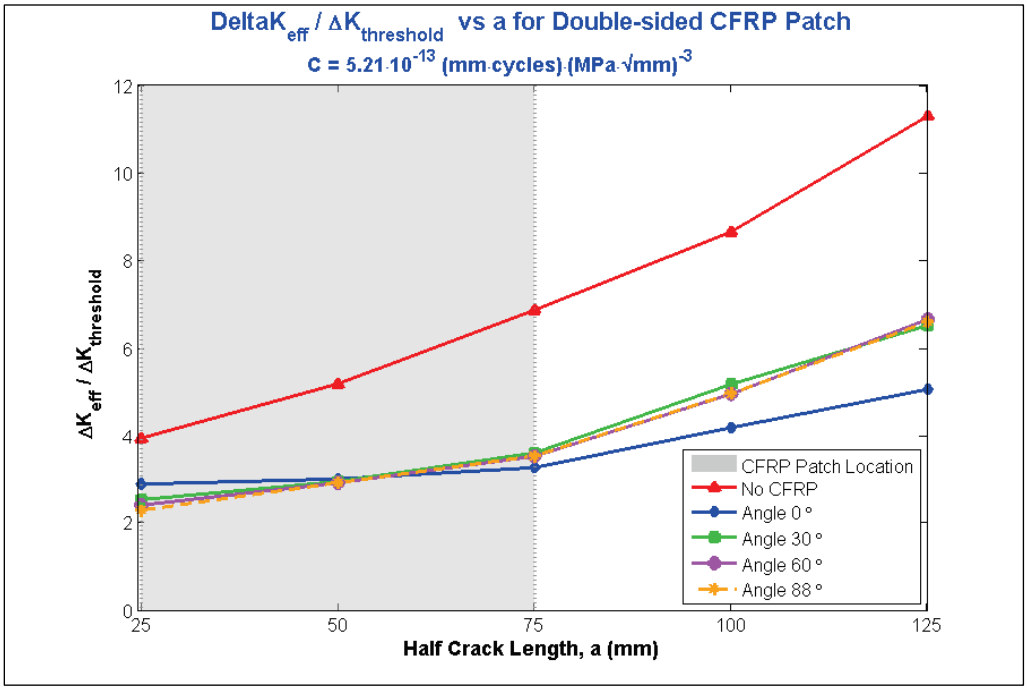

Figure 41. $\Delta K_{eff}/\Delta K_{threshold}$ vs. a for double-sided prestressed CFRP patch, $C = 5.21 \cdot 10^{-13}$ (mm·cycles)(MPa·√mm).

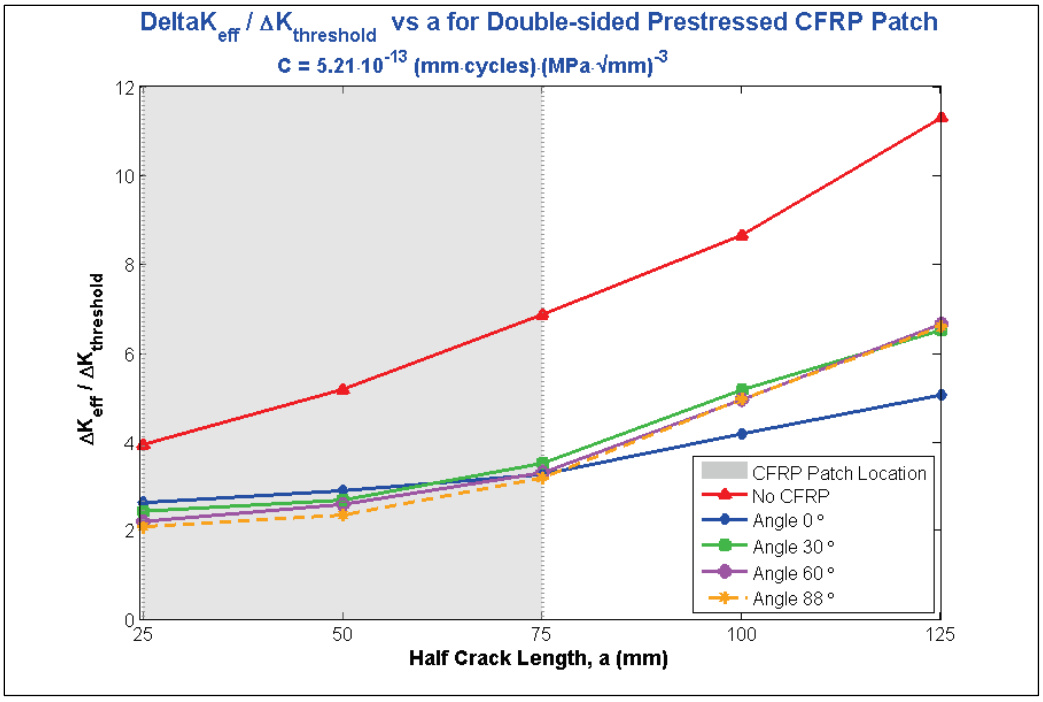

4.6 Adhesive Contours for Turbulent Flow (peel or no peel)

The water velocity, normal to the plate, was set to 10 mm/sec in the previously discussed analyses and it was based on a typical river flow velocity. The velocity profile used in the project in combination with the geometry of the FEM model resulted in laminar flow based on calculations of an open channel. However, another aspect of the effect of CFRP was the consideration whether the adhesive would fail during turbulent flows, thus, causing peeling of the CFRP. The von Mises failure criterion was used to define the failure of adhesive (yielding). Based on the adhesive material model, the yield stress was approximated as 30 MPa; therefore, if the von Mises stress exceeded 30 MPa, then the adhesive is said to have failed and the CFRP peeled.

Three different lengths of CFRP (and adhesive) were considered in junction with a new water velocity corresponding to turbulent flow (R_e = 10000). The three different lengths of CFRP signify gradual peeling of CFRP from its original installation. The difference between the three different adhesives and CFRP lengths is 75 mm. For these three models, a = 50 mm, which means that the crack ends coincide with the centers of the adhesive and CFRP strips. Von Mises stress contours for the adhesive for the three different strip lengths are shown in Figure 42. It is clear that

there is high stress concentration around the crack tips for all three cases, with more stresses observed in one of the patches than the other one. As the length of the CFRP strip reduces, the stresses appear to be concentrated more around the edges of the CFRP. However, less stresses are developed in the CFRP patches, because as the length of the CFRP patches reduces, it does not undergo large bending due to its proximity to the centerline of the plate, hence, the less observed stresses. Figure 43 shows the stress versus strain data obtained from the simulation superimposed on actual uniaxial material test data for Sika SIKADUR 30[1] epoxy (Riveros and Rosario 2013). The plot shows that the maximum strain was never exceeded in the simulations. However, the stress was slightly exceeded in some cases, implying that adhesive with higher strength might be needed for actual field applications. The reason for the stress-strain values not following the actual test data is because the plotted results from the numerical models are obtained at the element centroid, which is average of all values calculated at the Gauss points.

[1]SIKADUR 30, Sika, Australia. http://aus.sika.com/en/solutions_products/02/02a013/02a013sa05/02a013sa05100/02a013sa05102.html

Figure 42. Adhesive stress contours for turbulent flow.

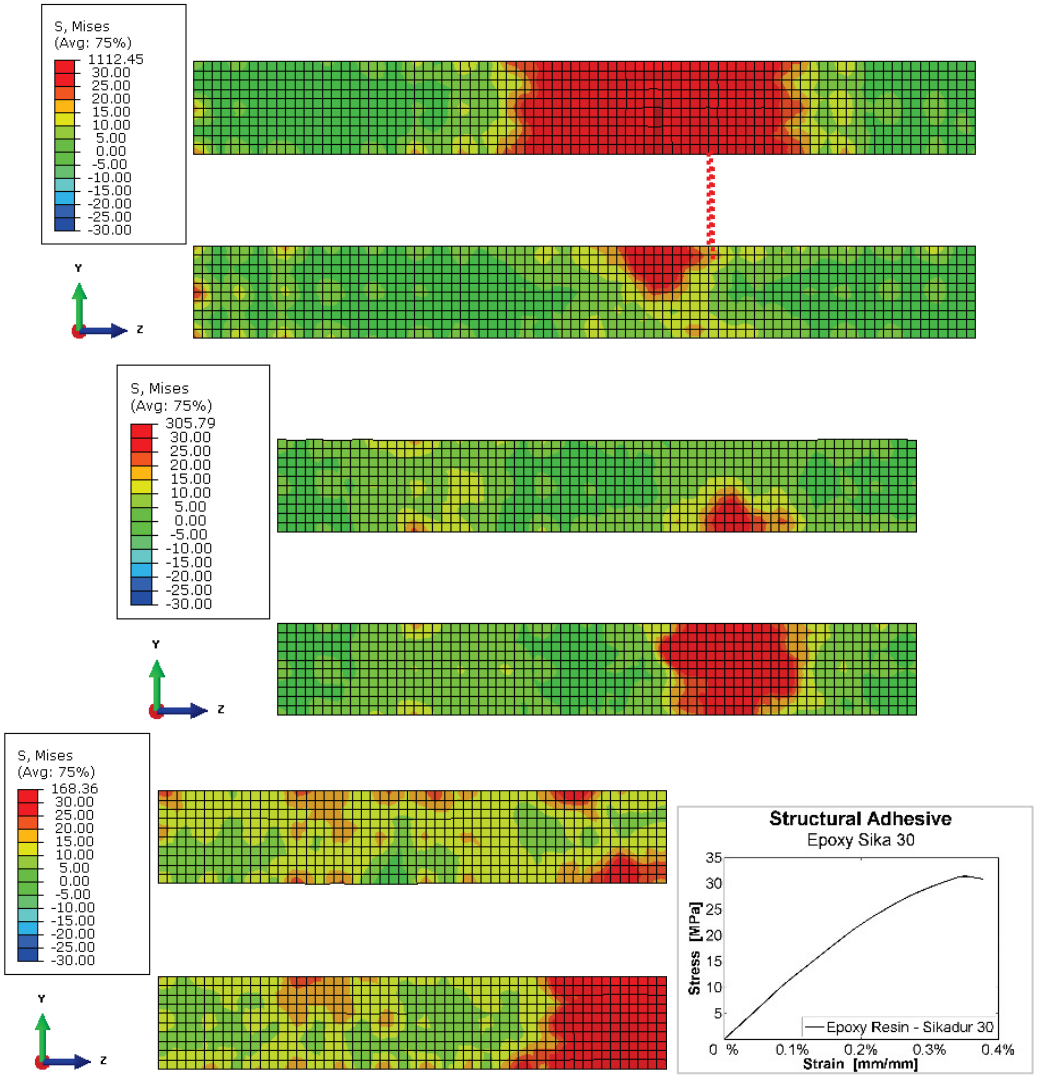

Figure 43. Adhesive stress-strain data for turbulent flow.

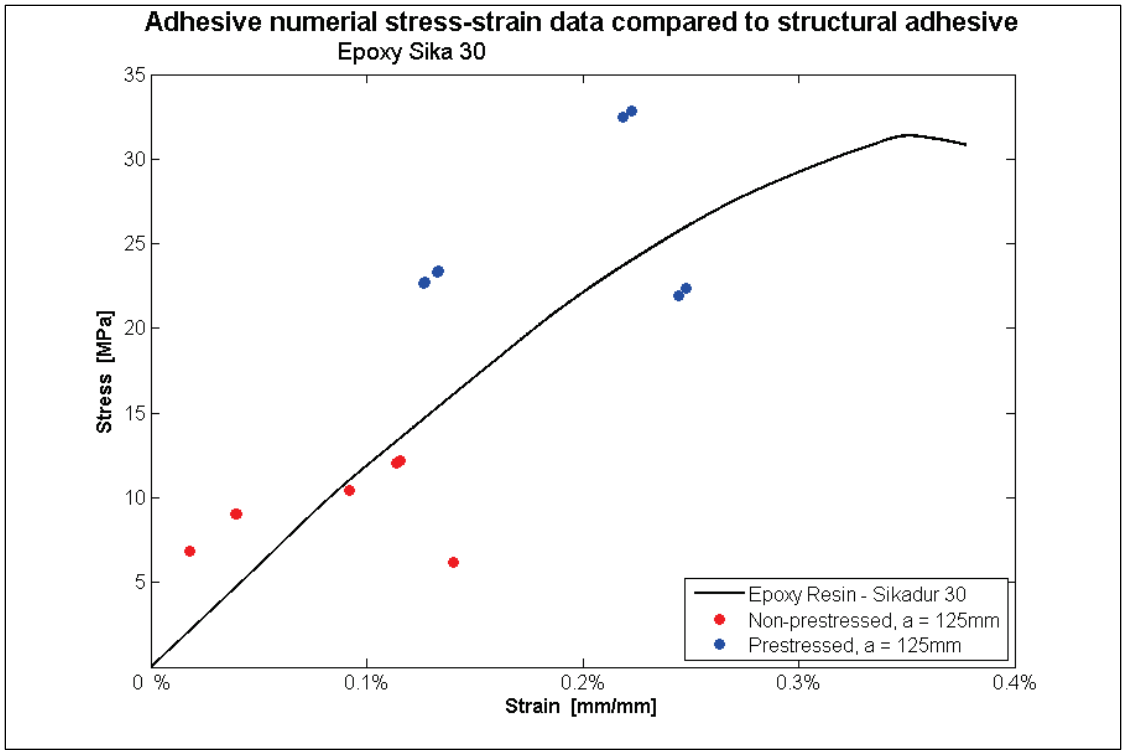

5 Conclusions

Fatigue cracks in steel structures are known to be a common nuisance, which could lead to catastrophic failures if left unrepaired. Although current repair specifications are applicable to fatigue design of steel bridges under Mode-I loading with a minor level of corrosion, their applicability to SHS is rather questionable. This is because SHS are often subjected to Mode-II and III, in addition to Mode-I, and are continuously exposed to harsh environmental conditions. Consequently, there is also significant uncertainty regarding the applicability of existing repair methods that are developed for the steel bridge industry for the repair of SHS. The uncertainty is further aggravated by the fact that existing steel bridge-based retrofits are often ineffective even when applied to steel bridges.

In this study, the use of CFRP patches for the fatigue repair of steel panels subjected to loading and boundary conditions that are representative of those of a miter gate have been investigated numerically. The studies have shown significant enhancement in fatigue life when CFRP is properly applied and debonding is avoided. The study includes the simulation of water impacting the panel using fluid structure interaction. The boundary conditions represent both open and closed conditions of the gate with varying water angles of attack including 0^{o}, 30^{o}, 60^{o}, and 88^{o}. The fatigue life assessment is conducted using the Paris Law for crack propagation analysis under both corrosive and non-corrosive environments. The investigated parameters include crack length, angle of impact (water velocity profile) or operation state of the gate, single-sided or double-sided CFRP patches, and CFRP prestressing.

Some of the main observations of this study are summarized as follows:

- CFRP-repaired plates show significant improvement over non-repaired plates.
- Single-sided CFRP introduce asymmetrical bending in the model, reducing the effectiveness of the retrofit.
- Double-sided CFRP repairs exhibit significant improvement over single-sided CFRP repairs, up to 2.7 times.

- Prestressing improves CFRP performance meaningfully. A low level of prestress (500 MPa) on average enhanced performance by 26%, up to 45% in some cases.
- Double-sided prestressed CFRP repairs exhibited the best performance, showing improvements of 5 times or greater compared to unrepaired models, and 2.5 to 3 times better results than single-prestressed and single-sided CFRP repairs.
- Double-sided CFRP repairs (both prestressed and non-prestressed) were significantly more efficient in reducing the crack propagation in comparison to unrepaired models and single-sided CFRP repairs.
- When crack length was at the edge or under the CFRP patch, the CFRP patch was more efficient in reducing the stress intensity factors, rather than when the crack had already propagated beyond the CFRP width.
- During the turbulent flow analysis, debonding around the crack is visible, as the stresses around the crack clearly exceed the yield stress of the adhesive.
- For turbulent flow, peeling of CFRP (due to the failing of adhesive) could become an issue, so appropriate preparation and installation is vital.
- High stress concentrations are shown to develop at the bottom boundary condition in the panel, where pintles are typically installed and are known to exhibit cracking.

6 Future work

The analysis conducted in this study showed the significant potential of using CFRP for the fatigue repair of miter gates. The numerical simulations provided very valuable insight on the most effective repair method for loading and boundary conditions that are representative of that of miter gate. Further analysis can be conducted to investigate other parameters as highlighted below.

- Larger range of prestressing could give better understanding of the optimal prestressing values so that a complete crack arrest can be achieved.
- Various water velocities ranging from laminar to turbulent flow could be included to further investigate peeling stresses and peeling velocities, and furthermore, to investigate the effect of peeling on stress intensity factors.
- Analytical evaluation can be conducted on crack propagations under combined modes, which can be a dominate factor in miter gate cracking.
- Analysis conducted on actual miter gate geometries that include all features of the gate (bolts, welds, residual stress field) will allow for more realistic assessment.
- Experimental evaluation of the various repairs can aid in understanding the full potential of this repair methodology and further calibration of the finite element models.
- Field application coupled with health monitoring can be viewed as a test bed for verifying the numerical and experimental results.

References

American Association of State Highway and Transportation Officials (AASHTO). 2012. *LRFD Bridge Design Specifications*. Washington, DC: American Association of State Highway and Transportation Officials. Sixth Edition.

ABAQUS Analysis Users Manual. 2011. *Linear Us – Up Hugoniot Form*. Version 6.11, Section 24.2.1. Dassault Systèmes.

ABAQUS Analysis Users Manua. 2011. *Formulation of Eulerian-Lagrangian Contact*. Version 6.11, Section 14.1.1. Dassault Systèmes.

ANSYS, Inc. http://www.ansys.com/ , Canonsburg, PA.

ASCE Committee on Composite Construction. 2006. *Task Group on Steel-FRP Composite Construction*. St. Louis, Missouri.

Bassetti, A., P. Liechti, and A. Nussbaumer. 1999. *Fatigue Resistance and Repairs of Riveted Bridge Members*. Espoo, Finland: 3rd International Symposium on Fatigue Design, Fatigue Design and Reliability.

Benmokrane, B., and H. Rahman. 1998. *Durability of Fibre Reinforced Polymer (FRP) Composites for Construction*. Universite' Sherbrooke: Department of Civil Engineering.

British Standards. 2012. BS 7910: Guide on Methods for Assessing hte Acceptability of Flaws in Metalic Structures.

Chue, C-H., L-C. Chang, J-S. Tsai. 1994. Bonded repair of a plate with inclined central crack under biaxial loading. *Composite Structures,* 28: 39-45.

Colombi, P., A. Bassetti, A. Nussbaumer. 2002. Crack growth induced delamination on steel members reinforced by prestressed composite patch. *Fatigue and Fracture Engineering Material Structure,* 26: 429-437.

Colombi, P., A. Bassetti, A. Nussbaumer. 2003. Crack Growth Induced Delamination on Steel Members Reinforced by Prestressed Composite Patch. *Fatigue and Fracture Engineering Material Structure,* 26: 59-66.

Como, A. and H. Mahmoud. 2013. Numerical evaluation of tsunami debris impact loading on wooden structural walls. *Engineering Structures*, 56: 1249–1261.

Dexter, R., H. Mahmoud, J. Padula, and G. Riveros. 2007. *Fitness-for-Purpose Evaluation of Hydraulic Steel Structures*. ERDC TR-07-15. Vicksburg, MS: U.S. Army Engineer Research Development Center, U.S. Army Corps of Engineers.

Duong, C., and C. Wang. 2004. On the Characterization of Fatigue Crack Growth in a Plate with a Single-Sided Repair. *J. of Engineering Materials and Technology*, 126(2): 192-198.

Haehnel, R. B., and S. F. Daly. 2002. *Maximum Impact Force of Woody Debris on Floodplain Structures*, Technical Report TR-02-2, Springfield, VA: U.S. Army Engineer Research and Development Center, U.S. Army Corps of Engineers.

Hansen, C., J. Schmidt, and B. Täljsten. 2007. *Strengthening of Old Metallic Structures in Fatigue with CFRP Materials*. Hong Kong, China: Asia-Pacific Conference on FRP in Structures (APFIS 2007).

Hosseini-Toudeshky, H., and B. Mohammadi. 2007. A simple method to calculate the crack growth life of adhesively repaired aluminum panels. *Composite Structures*, 79: 234–241.

Jiao, H., and X-L Zhao. 2004. CFRP Strengthened Butt-welded Very High Strength (VHS) Circular Steel Tubes. *Journal of Thin-Walled Structures,* 42: 963-978.

Jones, S., and S. Civjan S. 2003. Application of Fiber Reinforced Polymer Overlays to Extend Steel Fatigue Life. *Journal of Composites for Construction*, 7(4).

Kim, Y., and K. Harries. 2011. Fatigue behavior of damaged steel beams repaired with CFRP strips. *Engineering Structures,* 33: 1491-1502.

Liu, H., R. Al-Mahaidi, and X-L Zhao. 2009. Experimental Study of Fatigue Crack Growth Behaviour in Adhesively Reinforced Steel Structures. *Journal of Composite Structures,* 90: 12-20.

Mahmoud, H. and G. Riveros. 2013. Fatigue Repair of Steel Hydraulic Structures (SHS) using Carbon Fiber Reinforced Polymers (CFRP): Feasibility Study. ERDC/ITL TR-13-1. Vicksburg, MS: U.S. Army Engineer Research and Development Center, U.S. Army Corps of Engineers.

Maruyama, K. 1997. JCI Activities on Continuous Fibre Reinforced Concrete, Non-Metallic (FRP) Reinforcement for Concrete Structures. *J. C. Institute*: 3-12.

Mertz, D., J. Gillespie, M. Chajes, and S. Sabol. 2002. *The Rehabilitation of Steel Bridge Girders Using Advanced Composite Materials*. Final Report for NCHRP-IDEA Project 51.

Meier, U., and Betti R. 1997. *Recent Advances in Bridge Engineering – Advanced Rehabilitation, Durable Materials*, Non-destructive Evaluation and Management. EMPA. Switzerland.

Mirmiran A., M. Shahawy, A. Nanni, and V. Karbhari. 2004. *Bonded Repair and Retrofit of Concrete Structures Using FRP Composites - Recommended Construction Specifications and Process Control Manual*. Report 514. NCHRP.

Naboulsi, S., and S. Mall. 1996. Modeling of a cracked metallic structure with bonded composite patch using the three layer technique. *Composite Structures*, 35: 295-308.

Neale, K., and P. Labossiere. 1997. State-of-the-art Report on Retrofitting and Strengthening by Continuous Fibre in Canada. *J. C. Institute*: 25-39.

Paris, P., and F. Erdogan. 1963. A Critical Analysis of crack Propagation Laws. Trans. ASME, Ser. D. *Journal of Basic Engineering*, 85(4): 528-534.

Ramsden, J. D. 1993. *Tsunamis: forces on a vertical wall caused by long waves, bores, and surges on a dry bed*. PhD Dissertation, California Institute of Technology.

Riveros, G., and E. Arredondo. 2010. *Predicting Deterioration of Navigation Steel Hydraulic Structures with Markov Chain and Latin Hypercube Simulation*. ERDC/CHL CHETN-IX-24. Vicksburg, MS: U.S. Army Engineer Research Development Center, U.S. Army Corps of Engineers.

Riveros, G. A., and M. E. Rosario Perez. 2013. *Investigation of Available Constitutive Models and Nonlinear Experimental Data for Structural Epoxy Adhesives*. Under review, Vicksburg, MS: U.S. Army Engineer Research and Development Center, U.S. Army Corps of Engineers.

Schubbe, J., and S. Mall. 1999. Modeling of cracked thick metallic structure with bonded composite patch repair using three-layer technique. *Composite Structures*, 45: 185 - 193.

Shaat, A., D. Schnerch, A. Fam, and S. Rizkalla. 2004. *Retrofit of Steel Structures Using Fiber Reinforced Polymers (FRP): State-of-the-Art*. Washington, DC: Transportation research board (TRB) 83rd annual meeting.

Seo, D-C., and J-J. Lee. 2002. Fatigue crack growth behavior of cracked aluminum plate repaired with composite patch. *Composite Structures*, 57: 323–330.

Shield C., J. Hajjar, and K. Nozaka. (2004). *Repair of Fatigued Steel Bridge Girders with Carbon Fiber Strips*. Report No. MN/RC-2004-02. Minneapolis, MN.: M. D. o. Transportation. http://hdl.handle.net/11299/771.

SIMULIA. 2012. Coupled Eulerian-Lagrangian Analysis with Abaqus/Explicit, Retrieved from http://www.3ds.com/products/simulia/services/training-courses/course-descriptions/coupled-eulerian-lagrangian-analysis-with-abaqusexplicit/

Sun, C., J. Klug, and C. Arendt. 1996. Analysis of Cracked Aluminum Plates Repaired by Bonded Composite Patches. *AIAA Journal*, 34(2): 369-374.

Taljsten, B. 1997. Strengthening of Beams by Plate Bonding. *Journal of Materials in Civil Engineering*, 9(4): 206-212.

Tavakkolizadeh, M., and H. Saadatmanesh. 2003. Fatigue Strength of Steel Girders Strengthened with Carbon Fiber Reinforced Polymer Patch. *Journal of Structural Engineering*, 129(2): 186–196.

Thomas, J. 1978. FRP Strengthening - Experimental or Mainstream Technology? *Concrete International 20(6)*: 57-58.

Trask, D. 2000. Experimental and Numerical Investigation Into Fatigue Crack Propagation Models For 350WT Steel, DREA-CR-98-436. Dartmouth NS, Canada: Defense Research Establishment Atlantic.

Triantafillou, T. C. 1998. Shear Strengthening of Reinforced Concrete Beams Using Epoxy Bonded FRP Composites. *ACI Structural Journal*, 95(2): 107-115.

Umamaheswar, T., and R. Singh. 1999. Modelling of a patch repair to a thin cracked sheet. *Engineering Fracture Mechanics*, 62: 267 - 289.

Vatandoost, F. 2010. *Fatigue Behaviour of Steel Girders Strengthened with Prestressed CFRP Strips*. Civil Engineering, University of Waterloo. Masters of Science Thesis: 224.

Young, A., and D. Roore. 1992. Analysis of Patched and Stiffened Cracked Panels Using the Boundary Element Method. *Int. Journal of Solids and Structures,* 29(27).

Yue, Q., F. Peng, N. Zhang, and Y. X. Yang. 2004. *Experimental and Finite Element Studies on Deteriorated Steel Members Repaired with CFRP Sheets*. FRP Composites in Civil Engineering, CICE 2004 Adelaide, Australia, Proceeding of the Second International Conference on FRP Composites in Civil Engineering.